OBJECT SIZE EXTRACTION FROM IN-LINE HOLOGRAMS BY USING WIGNER-VILLE DISTRIBUTION

Porntip Chuamchaitrakool

A Thesis Submitted in Partial Fulfillment of the Requirements for the

Degree of Doctor of Philosophy in Laser Technology

Suranaree University of Technology

Academic Year 2017

การสกัดข้อมูลขนาดวัตถุจากอินไลน์ฮอโลแกรมโดยใช้
การกระจายวิกเนอร์-วิลล์

นางสาวพรทิพย์ เชื่อมชัยตระกูล

วิทยานิพนธ์นี้เป็นส่วนหนึ่งของการศึกษาตามหลักสูตรปริญญาวิทยาศาสตรดุษฎีบัณฑิต
สาขาวิชาเทคโนโลยีเลเซอร์
มหาวิทยาลัยเทคโนโลยีสุรนารี
ปีการศึกษา 2560

OBJECT SIZE EXTRACTION FROM IN-LINE HOLOGRAMS

BY USING WIGNER-VILLE DISTRIBUTION

Suranaree University of Technology has approved this thesis submitted in partial fulfillment of the requirements for the Degree of Doctor of Philosophy.
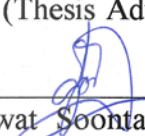
Thesis Examining Committee

_____

(Dr. Nuanwan Sanguansak)
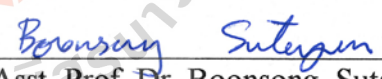
Chairperson

_____

(Prof. Dr. Joewono Widjaja)

Member (Thesis Advisor)

_____

(Dr. Siriwat Soontaranon)

Member

_____

(Assoc. Prof. Dr. Eckart Robert Schulz)

Member

_____

(Asst. Prof. Dr. Boonsong Sutapun)

Member

_____

(Asst. Prof. Dr. Panomsak Meemon)

Member

_____

(Asst. Prof. Dr. Worawat Meevasana)

_____

(Prof. Dr. Santi Maensiri)

Vice Rector for Academic Affairs

and Internationalization

Dean of Institute of Science

พรทิพย์ เชื่อมชัยตระกูล : การสกัดข้อมูลขนาดวัตถุจากอินไลน์ฮอโลแกรมโดยใช้การ
กระจายวิกเนอร์-วิลล์ (OBJECT SIZE EXTRACTION FROM IN-LINE HOLOGRAMS
BY USING WIGNER-VILLE DISTRIBUTION) อาจารย์ที่ปรึกษา : ศาสตราจารย์
ดร. ยูโวโน วิดจายา, 85 หน้า.

วิทยานิพนธ์นี้นำเสนอ วิธีการใหม่แบบไม่คำนวณซ้ำในการสกัดข้อมูลขนาดวัตถุ
จากอินไลน์ฮอโลแกรมโดยใช้การกระจายวิกเนอร์-วิลล์ (ดับเบิลยูวีดี) สมการคณิตศาสตร์
ของดับเบิลยูวีดีของอินไลน์ฮอโลแกรมวัตถุรูปทรงแท่งแสดงให้เห็นว่า ที่ตำแหน่งเท่ากับครึ่งหนึ่ง
ของความยาวฮอโลแกรม สัมประสิทธ์ของดับเบิลยูวีดีสองส่วน ปรากฏความสัมพันธ์เชื่อมโยงกัน
โดยตรงระหว่างข้อมูลขนาดวัตถุกับความถี่เฉพาะถิ่น คุณลักษณะสำคัญนี้ได้นำไปพัฒนาวิธีการ
สกัดข้อมูลขนาดวัตถุ แบบไม่อาศัยการคำนวณสร้างภาพย้อนกลับตามแบบดั้งเดิม และพบว่าข้อมูล
ขนาดวัตถุที่สกัดได้ ขึ้นอยู่กับความละเอียดของความถี่เชิงพื้นที่ของดับเบิลยูวีดี ดังนั้นเพื่อให้ข้อมูล
ขนาดวัตถุมีความถูกต้องยิ่งขึ้น ความยาวของฮอโลแกรมได้ยืดออกด้วยเทคนิคการพลิกกลับ
และทำซ้ำ (เอฟอาร์ที) ความเป็นไปได้ของวิธีการสกัดข้อมูลขนาดวัตถุที่นำเสนอทั้งแบบใช้
เอฟอาร์ทีและไม่ใช้เอฟอาร์ที พิสูจน์ได้จากการยืนยันทางการทดลอง ผลการทดลองพบว่า ความ
ถูกต้องของข้อมูลขนาดวัตถุเพิ่มสูงขึ้นเมื่อใช้เอฟอาร์ที ซึ่งวิธีการสกัดขนาดวัตถุที่นำเสนอนี้
เหมาะสำหรับอินไลน์ฮอโลแกรมที่บันทึกด้วยตัวตรวจรู้ขนาดเล็ก

สาขาวิชาฟิสิกส์   ลายมือชื่อนักศึกษา_พรทิพย์ เชื่อมชัยตระกูล_
ปีการศึกษา 2560   ลายมือชื่ออาจารย์ที่ปรึกษา_____
                                     ลายมือชื่ออาจารย์ที่ปรึกษาร่วม Hiroyuki Yoshimura

PORNTIP CHUAMCHAITRAKOOL : OBJECT SIZE EXTRACTION
FROM IN-LINE HOLOGRAMS BY USING WIGNER-VILLE
DISTRIBUTION. THESIS ADVISOR : PROF. JOEWONO WIDJAJA,
Ph.D. 85 PP.

IN-LINE HOLOGRAPHY/WIGNER-VILLE DISTRIBUTION/OBJECT SIZE
MEASUREMENT/ROD-SHAPED OBJECT

A non-iterative method for extracting object size from an in-line hologram by
using Wigner-Ville distribution (WVD) is proposed in this thesis. To implement the
proposed method, the mathematical expression of the WVD of a simplified in-line
hologram of a rod-shaped object is first derived. From the mathematical derivation of
the WVD of the hologram, it is found that two coefficients of the WVD output at the
half length of the holograms give a direct relationship between the object size and the
local frequencies. By taking this property into account, the WVD can give
information on the object size. The object size calculated by the proposed method is
found dependent upon the spatial-frequency resolution of the WVD. This causes the
accuracy of the object size measurement to directly rely on the resolution of the CCD
sensor being used for the hologram recording. In order to improve the measurement
accuracy of the proposed object sizing method, the hologram length is extended by
using a flip and a replication process. The feasibilities of the object sizing method
with and without using a flip and replication technique (FRT) are experimentally
verified. The results show that the object size can be precisely extracted by using the

WVD. The accuracy of object size measurement at the shorter recording distance is able to be improved by using the FRT. Thus, the proposed method is suitable for sizing in-line object holograms recorded by low-resolution image sensors.

School of Physics

Academic Year 2017

Student's Signature พรทิพย์ เชื่อมชัยตระกูล

Advisor's Signature

Co-advisor's Signature Hiroyuki Yoshimura

ACKNOWLEDGEMENTS

CONTENTS

CONTENTS (Continued)

LIST OF TABLES

LIST OF FIGURES

LIST OF FIGURES (Continued)

LIST OF FIGURES (Continued)

CHAPTER I

INTRODUCTION

1.1 Background

Digital in-line holography (DIH) is an optical imaging technique using a coherent wave as a light source. The principle of this technique is based on the in-line holography invented by Denis Gabor in 1948 and relies on advanced technologies of the image sensor (Thompson, 1974; Schnars and Jüptner, 1994; Hariharan, 1996). The DIH is potent for sizing and tracking both three-dimensional small opaque or semi-transparent particles and microorganisms. This is because of the distinguishing properties of the DIH, namely simple alignment, noncontact, noninvasiveness, and label-free tool for metrology.

For the past decade, the tracking and the profiling of microscale objects by using the DIH have been conducted not only for observing static behaviors of particles but also the dynamic ones. Flow of the red blood cells in humans is one of medical applications. Characteristics of the flow were investigated and used to diagnose the circulatory system (Choi and Lee, 2009; Moon, Javidi, Yi, Boss and Marquet, 2012). In order to understand heat transfer during combustion, aerospace engineers use the DIH to investigate flow details and the size of aluminum drops within the plume of the solid propellant (Guildenbecher, Cooper, Gill, Stauffacher, Oliver and Grasser, 2014). By taking the noninvasive property, the DIH has been

employed to study motility and growth of microorganisms in biology (Carl, Kemper, Wernicke and Von Bally, 2004; Javidi,Moon, Yeom and Carapezza, 2005; Lee, Seo, Choi and Sohn, 2011). For reducing time consumed by the conventional protocol in monitoring the drinking water resources to prevent serious health crisis, the DIH was employed to identify parasitic protozoan *Giardia lamdia* cysts among two similar organisms (Mallahi, Minetti and Dubois, 2013). In zoology, morphological features of bull's sperms were studied by using the DIH because it would not alter a specimen's characteristics (Merola, Miccio, Memmolo, Di Caprio and Galli, 2013). The DIH is also able to give a high accuracy of sizing particles with high aspect ratio such as fibers or needle-shaped particles. As a result, chemical engineers have used the DIH for solving a focusing problem of conventional two-dimensional imaging systems in monitoring particle crystallization (Darakis, Khanam, Rajendran, Kariwala, Naughton, and Asundi, 2010; Khanam, Rahman, Rajendran, Kariwala and Asundi, 2011). Recently, DIH has also been used for understanding the infection process caused by rod-shaped bacteria (Moon, Yi and Javidi, 2010; Kemper *et al.*, 2013). In order to study morphology and biochemistry of live specimen for selecting the best spermatozoa for injecting into oocytes, the DIH was used in combination with high-specific Raman spectroscopy (Ferrara, Angelis, Luca, Coppola, Dale and Coppola, 2016).

The DIH is a two-step imaging process. The first process records an interference pattern of a plane reference wave and waves diffracted by the particles. When this interference pattern is captured by using an image sensor based on the complementary metal-oxide-semiconductor (CMOS) or a charge-coupled device (CCD) technology, a digital hologram is generated in which size and position

information of the particles being studied is encoded. Image capture is followed by the image reconstruction. This is done by solving numerically the Fresnel diffraction integral (Schnars and Jüptner, 1994; Goodman, 1996). Since the position of the particle is not known in advance, a set of images must be reconstructed by using different impulse responses of light propagation through free space. Sharpness of the reconstructed images is then quantitatively assessed to obtain the best focus image plane. Thus, the numerical reconstruction can be considered as an analogue of the conventional optical method. Owing to its iterative nature, this reconstruction process is computationally intensive. Although an angular spectrum method can be used to reduce computational time by directly generating a transfer function of free-space light propagation, the process of assessing focus quality from the whole reconstructed images remains unsolved (Kim and Lee, 2007). Finally, the object size is measured from the reconstructed image with the best focus.

To overcome the drawback of the conventional numerical reconstruction, wavelet transform (WT), which is a joint space-frequency signal representation has been proposed (Buraga-Lefebvre, Coëtmellec, Lebrun and Özkul, 2000; Soontaranon, Widjaja and Asakura, 2002, 2008; Widjaja and Soontaranon, 2009). The advantage of this analysis method is that the axial position of particles can be directly determined without the process of image reconstruction and evaluation. This was implemented by taking iterative correlations between the hologram signal and a bank of daughter wavelets, which have a frequency response similar to a band-pass filter. The daughter wavelet has been generated by using a spherical wave function with an axial distance of the wave propagation for its dilation (Buraga-Lefebvre, Coëtmellec, Lebrun and Özkul, 2000). Instead of treating the diffraction process from the view point of the

WT, Soontaranon *et al.* used a Morlet wavelet as the mother wavelet (Soontaranon, Widjaja and Asakura, 2002, 2008; Widjaja and Soontaranon, 2009). This proposed method has an advantage over the previous approach in that the dilation factor does not depend on the axial distance. Recently, Widjaja and Chuamchaitrakool used Wigner-Ville distribution (WVD) to overcome the iterative computation of the WT (Widjaja and Chuamchaitrakool, 2013). The main advantage of using the WVD is that besides employing a simple analyzing window that is the original itself, the WVD output coefficients provide local spatial-frequency of the fringe holograms. Their research demonstrated experimentally the measurement of the object position from the in-line holograms by calculating the rate of change of the local spatial-frequency of the WVD output.

1.2   Significance of the Study

With growing interest in studying rod-shaped particles and microorganisms (Black, McQuay and Bonin, 1996; Javidi *et al.*, 2005; Kemper *et al.*, 2013) and due to the usefulness of the WVD in tracking objects from in-line holograms, this research work extends the use of the WVD for sizing rod-shaped objects. The sizing method has three major advantages. Firstly, the object size can be directly calculated from the local spatial-frequencies occurred at the half length of the spatial axis in the WVD plane. Secondly, its computation is faster and simpler, because it does not require the image reconstructions and the focus quality assessments. Thirdly, a single computation of the WVD can be used not only for tracking and sizing particles, but it can also directly reconstruct the particle images.

1.3   Research Objectives

1.3.1 To derive a mathematical expression of the WVD of the in-line hologram of the rod-shaped object.

1.3.2 To extract the size of the rod-shaped objects from the holograms by using the WVD.

1.3.3 To verify feasibility of the proposed method.

1.4   Scope and Limitation of the Study

1.4.1 The proposed particle sizing method is verified experimentally.

1.4.2 A one-dimensional rod-shaped particle is used as the test object.

1.4.3 Size measurements by using the proposed particle sizing method are compared with those obtained from using the conventional numerical reconstruction.

1.4.4 Measurement performance is theoretically studied.

1.5   Organization of the Thesis

The remainder of the thesis is organized as follows. Chapter II is devoted to providing the theoretical background of in-line holography and the WVD. In Chapter III, the WVD of the in-line hologram of a rod-shaped particle is mathematically derived. The particle sizing by using the derived WVD coefficients is described. Finally, improvement of the measurement accuracy of the proposed sizing method by using a flip and replication technique (FRT) and the measurement performance are

discussed. Chapter IV discusses the experimental verifications of the proposed particle sizing method. Conclusions of the thesis are presented in Chapter V.
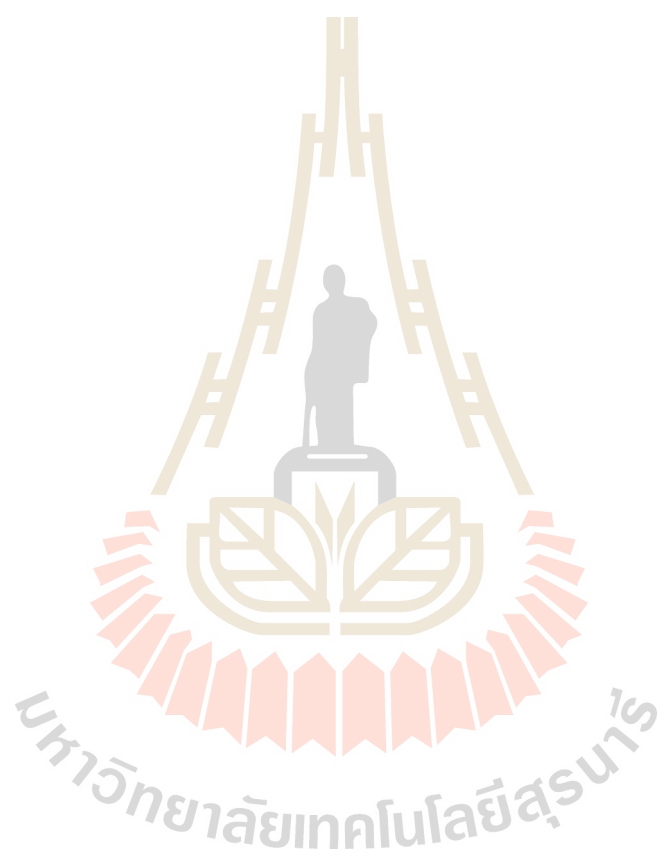
CHAPTER II

THEORY

The theory of digital in-line holography is reviewed in this chapter. Encoding of 3-D information of a rod-shaped particle in an in-line hologram is mathematically described. The property of the WVD is discussed by analyzing a cosine chirp signal.

2.1   Digital In-Line Holography

Development of holography has made significant progress since Schnars and Jüptner first used a CCD camera directly connected to a computer to digitally record interference patterns in 1994. Hologram reconstruction was then done by using a numerical computation. By this means, digital holography was named after their work (Schnars and Jüptner, 2005).

According to the geometries of recording setups, there are two types of digital holography, namely digital in-line holography (DIH) and digital off-axis holography. The DIH setup depicted in Figure 2.1(a) shows that after spatial filtering, a laser beam is expanded by a collimating lens placed behind a pinhole at a distance of its focal length. An illumination of particulate objects inside a test chamber by the collimated plane wave causes an interference between the waves diffracted by the objects and the reference wave. Recording of this interference pattern by using a CCD image sensor gives an in-line hologram. In Figure 2.1(b), the collimated beam is split

into two beams that are the reference and the object waves, respectively. This setup

provides flexibility in manipulating the reference beam. The two waves are interfered

on a CCD image sensor by using a beam combiner.
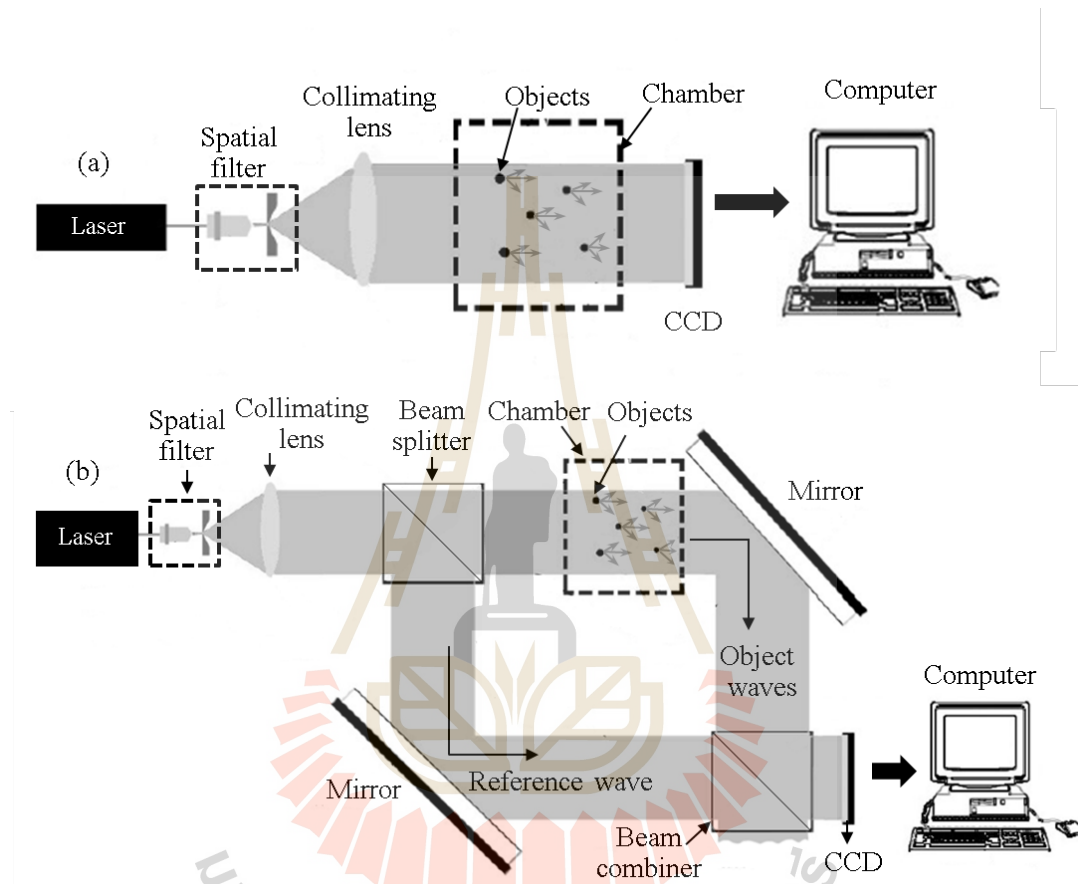
Figure 2.1 Optical setups of (a) digital in-line and (b) digital off-axis holographies,

respectively.

In the conventional numerical reconstruction method, the Fresnel diffraction

integral of the recorded holograms is calculated to extract object information. Figure

2.2 shows a schematic relation of the hologram $U_1(\xi,\eta)$ and its reconstructed fields

$U_2(x,y)$, respectively. The integration is implemented by convolving the hologram

$U_1(\xi,\eta)$ and the impulse response of free-space propagation $h(x,y;z_n)$ (Goodman, 1996).
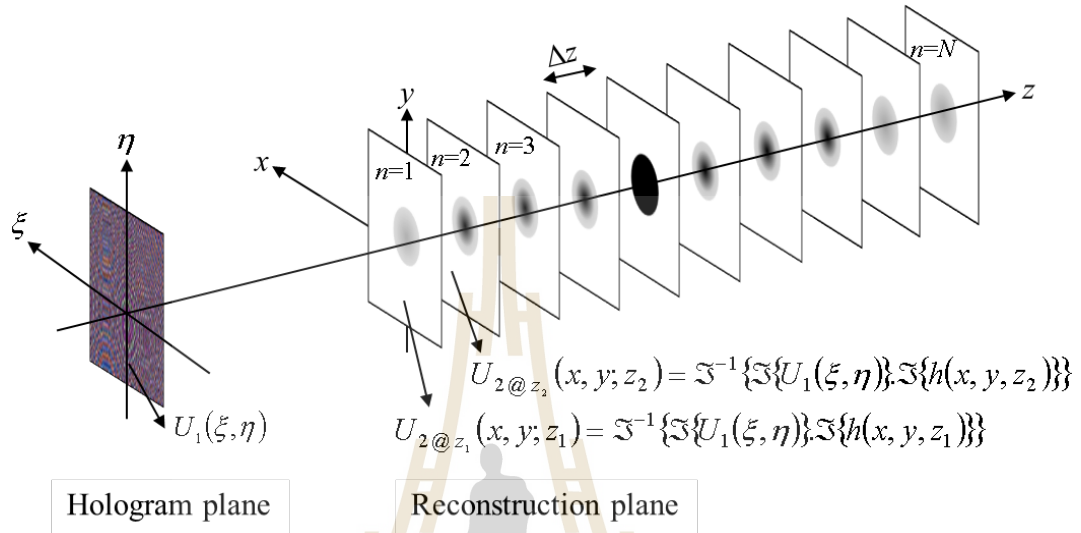
Figure 2.2 Numerical reconstruction by using the Fresnel diffraction integral.

$$U_{2@z_n}(x,y) = \iint U_1(\xi,\eta)h(x-\xi, y-\eta; z_n)d\xi d\eta, \qquad (2.1)$$

where

$$h(x,y;z_n) = \frac{e^{j\frac{2\pi}{\lambda}z_n}}{j\lambda z_n} \exp\left[\frac{j\pi}{\lambda z_n}(x^2 + y^2)\right]. \qquad (2.2)$$

According to signal processing, the convolution can be implemented by using fast Fourier transform

$$U_{2@z_n}(x,y;z_n) = \mathfrak{I}^{-1}\{\mathfrak{I}\{U_1(\xi,\eta)\}.\mathfrak{I}\{h(x,y,z_n)\}\}, \qquad (2.3)$$

where $\mathfrak{I}$ and $\mathfrak{I}^{-1}$ stand for the Fourier transform and the inverse Fourier transform operators, respectively. Since object positions are unknown, the numerical reconstruction is done for different axial distances z_n with a spacing of Δz.

A focus quality of each reconstructed particle image is then quantitatively assessed for the best focus, which indicates the actual position of the particle (Langehanenberg, Kemper, Dirksen and Bally, 2008). In case of multiple-particle tracking, further processes are needed to assist the sharpness evaluation. In order to get the best positions of particles, besides investigating a variation of peak intensities along a longitudinal distance, averaging and polynomial curve-fitting algorithms are adopted to account for errors (Yu, Hong, Liu, Cross, Haynie and Kim, 2014). Therefore, the conventional numerical reconstruction method employs a complex process, and intensive computations.

2.2 Digital In-Line Hologram of a Rod-Shaped Particle

In order to study properties of a hologram of a rod-shaped particle, recording of in-line particle holograms is done by using the optical setup illustrated in Figure 2.3. A coherent plane wave with an operating wavelength λ is used to illuminate the rod-shaped particle with a diameter of $2a$. An interference pattern between the wave diffracted by the particle and the directly transmitted plane wave is formed on a CCD image sensor placed at the distance z from the particle. The recorded hologram, which contains a symmetrical interference pattern with respect to the x-axis, can be mathematically expressed as (Tyler, 1976)

$$I(x) = \left\{ 1 + \frac{4a^2}{\lambda z} \left[\frac{\sin\left(\frac{2\pi ax}{\lambda z}\right)}{\frac{2\pi ax}{\lambda z}} \right]^2 - \frac{4a}{\sqrt{\lambda z}} \cos\left(\frac{\pi x^2}{\lambda z} - \frac{\pi}{4}\right) \left[\frac{\sin\left(\frac{2\pi ax}{\lambda z}\right)}{\frac{2\pi ax}{\lambda z}} \right] \right\} \mathrm{rect}\left(\frac{x}{2L}\right), \quad (2.4)$$

where $2L$ is the length of the hologram signal.
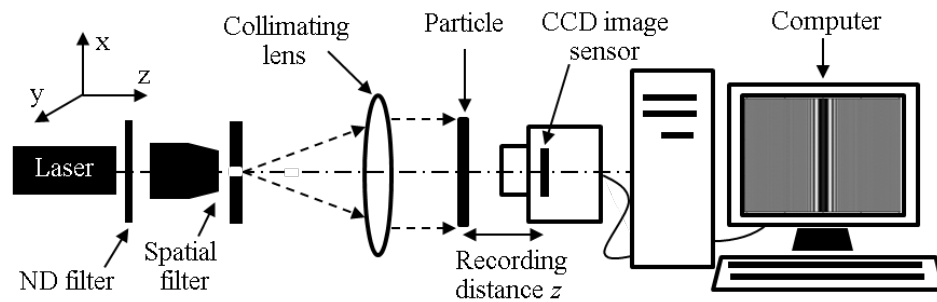
Figure 2.3 Optical setup of DIH for generating in-line holograms.

In Eq. (2.4), the first term represents the background intensity, while the second term is the square of the diffracted wave. Its amplitude is so small that it can be neglected in information extraction. The third term is a modulation of a cosine chirp signal by a sinc function, which encodes the desired particle information. Since the sinc function represents the diffraction pattern of the rod-shaped particle, width of its main lobe is determined by the particle size a. Whereas the frequency of the cosine chirp signal is inversely proportional to the recording distance z.

Figure 2.4(a) shows a typical hologram of the rod-shaped particle with the diameter $2a = 100$ µm, which was simulated by using Eq. (2.4) at a recording distance $z = 200$ mm and the wavelength $\lambda = 543.5$ nm with the length $2L = 8.30$ mm. Figure 2.4(b) is the 1-D intensity transmittance scanned along the horizontal axis of the hologram with a dc removal. The signal shows that as the position x is longer, the frequency of the cosine chirp becomes higher. The maximum amplitude of the signal is caused by the main lobe of the sinc function. Thus, it is apparent that the third term of Eq. (2.4) is the dominant signal in the in-line particle holograms.
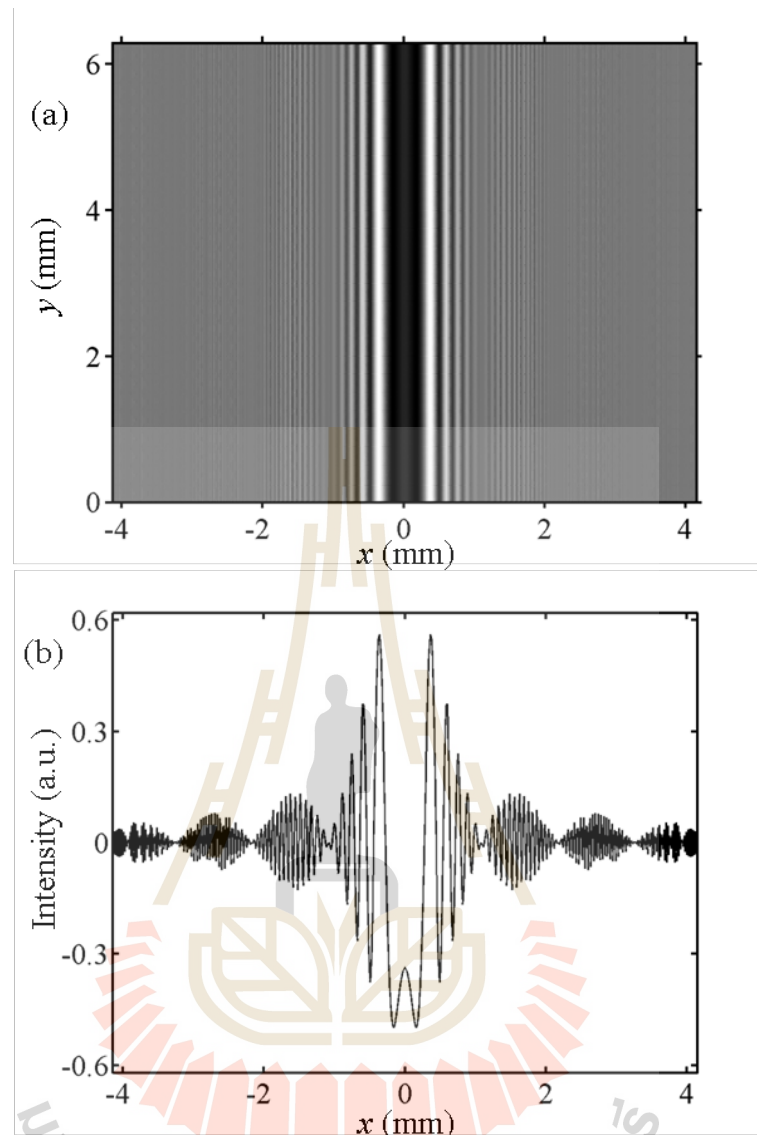
Figure 2.4 (a) Simulated in-line hologram of the rod-shaped particle with diameter $2a = 100$ μm produced at the recording distance $z = 200$ mm by using coherent light with a wavelength $\lambda = 543.5$ nm and (b) its intensity transmittance with dc removal.

2.3 Wigner-Ville Distribution

Wigner-Ville distribution (WVD) is a joint space-frequency signal representation, which has been widely used for analyzing non-stationary signals

(Boashash, 1988). In comparison with the Wigner distribution function, the WVD is free from frequency artifacts (Hlawatsch, 1984; Widjaja, Uozumi, Ushizaka and Asakura, 1992). The WVD of an analytic signal $g_a(x)$ is mathematically defined as the Fourier transform of the instantaneous autocorrelation $g_a(x+\xi/2)g_a^*(x-\xi/2)$ (Boashash, 1988)

$$W_{g_a}(x, f_x) = \int_{-\infty}^{\infty} g_a(x+\xi/2)g_a^*(x-\xi/2)\exp(-j2\pi f_x \xi)d\xi. \qquad (2.5)$$

The WVD output gives information on how the local spatial-frequency f_x varies with the position x. In order to understand the WVD properties, an analysis of a cosine chirp signal given by

$$g(x) = \cos\left(\frac{\pi x^2}{\lambda z}\right)\text{rect}\left(\frac{x - L/2}{L}\right) \qquad (2.6)$$

is considered.

Figure 2.5 shows a plot of the signal with $\lambda = 543.5$ nm, $z = 300$ mm and $L = 4.15$ mm with the number of pixels $N = 320$. The plot depicts a characteristic of the cosine chirp whose spatial frequency becomes higher as the position x increases. By using the Hilbert transform, an analytic expression of Eq. (2.6) can be written as

$$g_a(x) = \exp\left(\frac{j\pi x^2}{\lambda z}\right)\text{rect}\left(\frac{x - L/2}{L}\right). \qquad (2.7)$$

By taking the rectangular function into account, WVD of Eq. (2.7) can be written as

$$W_{g_a}(x, f_x) = \int_{-(L-2|x-L/2|)}^{(L-2|x-L/2|)} \exp\left[\frac{j\pi}{\lambda z}\left(x + \frac{\xi}{2}\right)^2\right]\exp\left[\frac{-j\pi}{\lambda z}\left(x - \frac{\xi}{2}\right)^2\right]\exp(-j2\pi f_x \xi)d\xi$$

$$= \int_{-(L-2|x-L/2|)}^{(L-2|x-L/2|)} \exp\left(\frac{2j\pi\xi x}{\lambda z} - j2\pi f_x \xi\right)d\xi. \qquad (2.8)$$
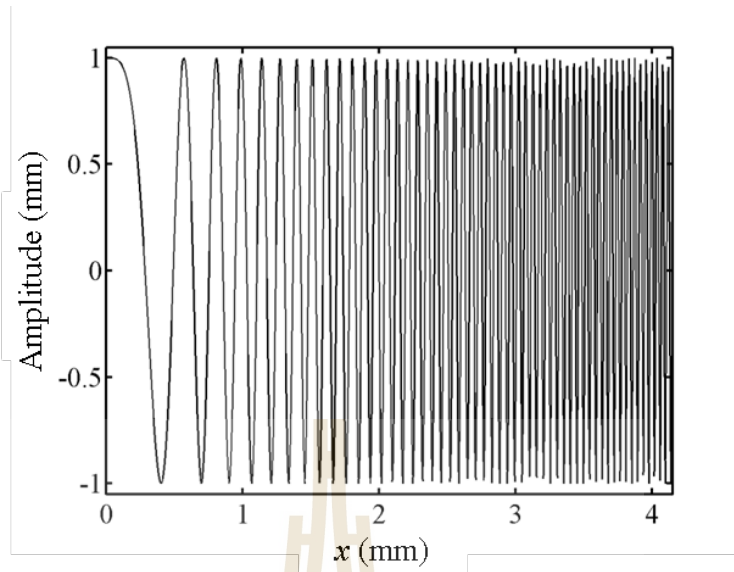
Figure 2.5 A plot of Eq. (2.6) for given parameters of $\lambda = 543.5$ nm, $z = 300$ mm

and $L = 4.15$ mm.

The integration result of Eq. (2.8) is equal to

$$W_{g_a}\left(x,f_x\right) = \frac{\exp\left[2j\pi\left(L-2\left|x-\frac{L}{2}\right|\right)\left(f_x-\frac{x}{\lambda z}\right)\right] - \exp\left[-2j\pi\left(L-2\left|x-\frac{L}{2}\right|\right)\left(f_x-\frac{x}{\lambda z}\right)\right]}{j2\pi\left(f_x-\frac{x}{\lambda z}\right)}$$

$$= 2\left(L-2\left|x-\frac{L}{2}\right|\right)\text{sinc}\left[2\left(L-2\left|x-\frac{L}{2}\right|\right)\times\left(f_x-\frac{x}{\lambda z}\right)\right]. \tag{2.9}$$

Equation (2.9) reveals that the output of the WVD of the cosine chirp signal is a

modulation of the 2-D sinc function of the space and the spatial frequency by the

triangular function. The peaks of the two functions coincide at $x = L/2$. Since the

spatial frequency of the sinc function is given by $x/\lambda z$, the modulation result gives

information of the instantaneous spatial frequency of the cosine chirp. This is the

important property of the WVD in signal analysis. In order to verify the above

derivation, the WVDs of the cosine chirp shown in Figure 2.5 calculated by using Eq. (2.6) and Eq. (2.9). They are plotted in Figure 2.6.
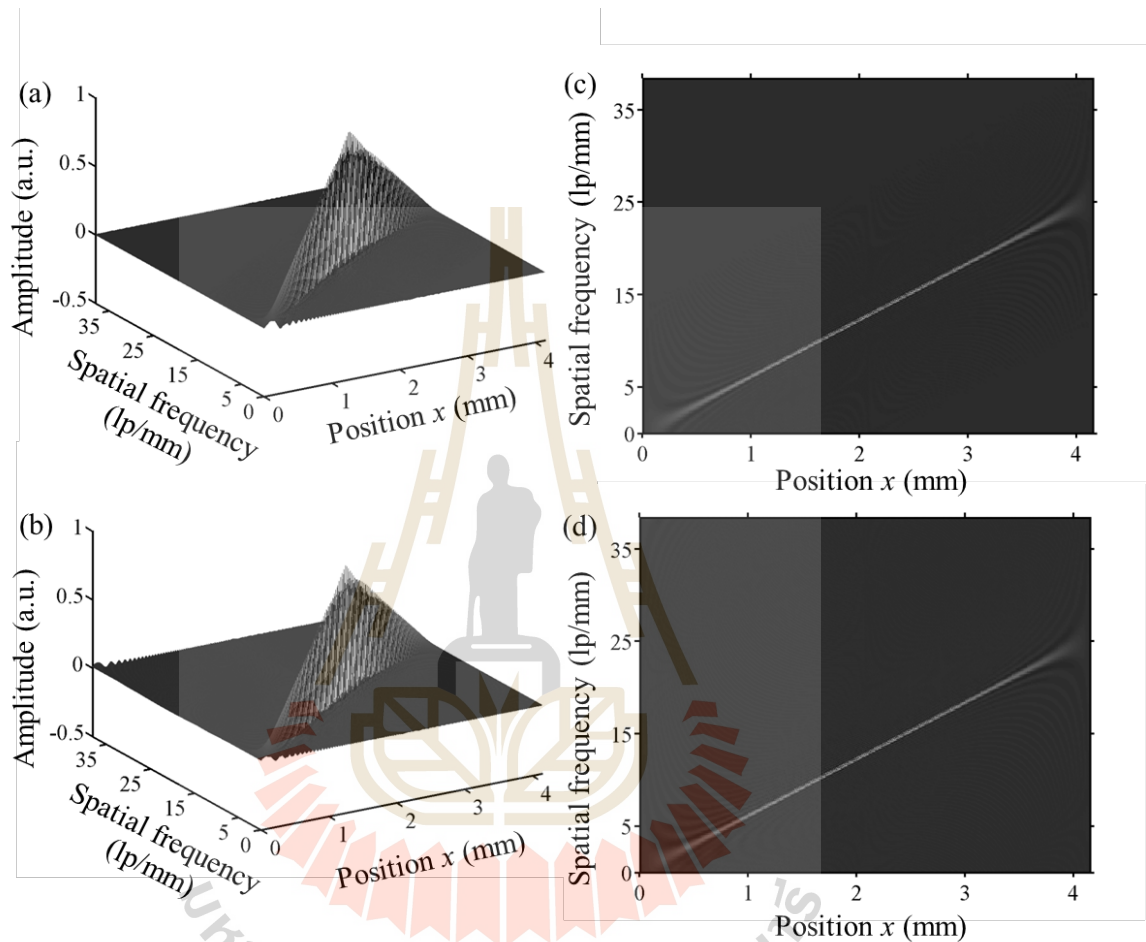
Figure 2.6 The WVDs of the cosine chirp shown in Figure 2.5. 3-D plots of (a) Eq. (2.9) and (b) WVD of Eq. (2.6). Top views of (c) Figure 2.6(a) and (d) Figure 2.6(b).

In Figure 2.6, the x and the y axes are the position x and the spatial frequency f_x, respectively. The z axis in the 3-D plot corresponds to the amplitude of the WVD coefficients. Here, the maximum and minimum amplitude values are represented by the white and the black color pixels, respectively. Figure 2.6(a) is the 3-D plot of the

WVD calculated by using Eq. (2.9), while Figure 2.6(b) is the WVD result of Eq. (2.6). Their top views are shown in Figures 2.6(c) and (d), respectively. It is obvious that certain WVD coefficients have triangular amplitude variation. They are distributed along a diagonal line with a slope $1/\lambda z$ in the WVD plane. The comparison of the plots validates the derivation of Eq. (2.9).

CHAPTER III

WVD OF IN-LINE HOLOGRAMS

This chapter discusses the extraction of particle size from in-line holograms by using the WVD. The first section begins with the discussion of the characteristics of the WVD of in-line holograms. In order to have better insight into the WVD, its mathematical expression is derived and verified. The mathematical result is applied to the particle sizing method. In order to improve the accuracy of the particle size measurement, a flip and replication technique is subsequently described. In the last section, measurement performance of the proposed particle sizing method is theoretically studied.

3.1 WVD of In-Line Holograms

The WVD of the in-line hologram of a rod-shaped particle shown in Figure 2.4(b) is illustrated in Figure 3.1. This WVD output gives similar result as Figure 2.6 in that the WVD coefficients are concentrated along the instantaneous frequency $x/\lambda z$ with the positive slope. Since the slope is inversely proportional to the particle position, the steepness of the slope can be used to give quick information of the particle depth, such that the steeper the slope, the closer the particle to the image sensor. In addition, the slope is positive, because the local spatial-frequency of the cosine chirp function of the hologram fringe in Eq. (2.4) becomes higher as the spatial

position increases. Since the WVD provides information of the local spatial-frequency f_x, the measurement of the rate of change of the spatial frequency of the WVD along the diagonal direction can be used to extract the position of the particle (Widjaja and Chuamchaitrakool, 2013).
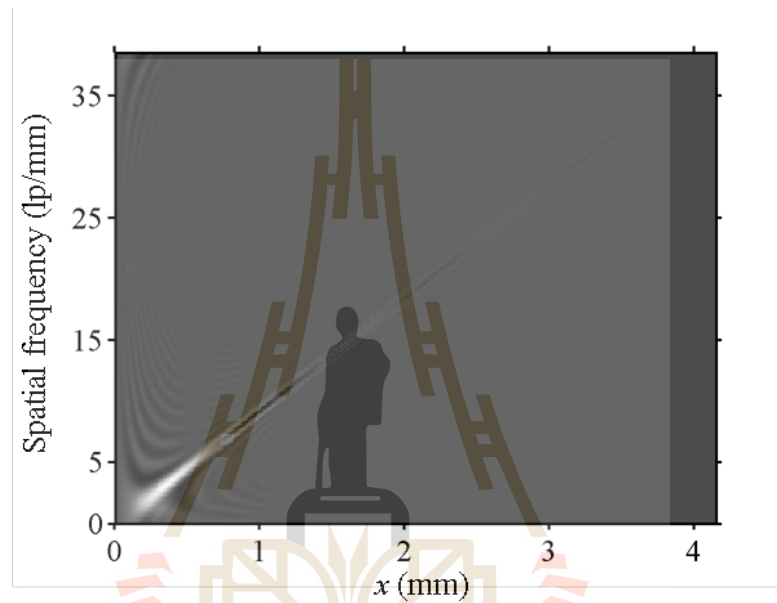
Figure 3.1 Plot of the WVD of the hologram signal along the positive *x*-axis shown

in Figure 2.4(b) with $L = 4.15$ mm.

In order to gain better insight into the WVD output of in-line particle hologram shown in Figure 3.1, the mathematical expression of the WVD is investigated. The hologram signal is simplified by considering only the third term of Eq. (2.4) along the positive direction of the *x*-axis as

$$I(x) = \cos\left(\frac{\pi x^2}{\lambda z} - \frac{\pi}{4}\right)\left[\frac{\sin\left(\frac{2\pi a x}{\lambda z}\right)}{\frac{2\pi a x}{\lambda z}}\right]\text{rect}\left(\frac{x - \frac{L}{2}}{L}\right). \tag{3.1}$$

The simplification is justified, because as discussed in Section 2.2, the third term is the dominant signal in-line hologram. It is a well-known fact that the analytic expression of the sinc function in Eq. (3.1) is difficult to express. Thus, the sinc function is approximated with a product of cosine functions (Morrison, 1995)

$$\mathrm{sinc}(2f_0 x) = \prod_{r=1}^{R} \cos\left(\frac{2\pi f_0 x}{2^r}\right), \tag{3.2}$$

where R denotes the number of the cosine terms and $f_0 = a/\lambda z$. Figure 3.2 shows the plots of the original sinc function compared with its approximations with $R = 3$ and $R = 5$.
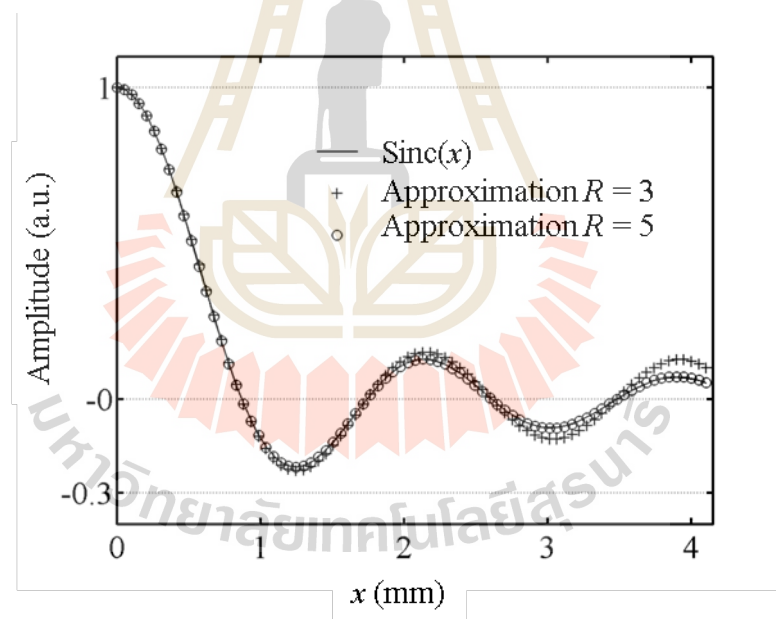
Figure 3.2 Plots of the sinc function and its approximations by using $R = 3$ and $R = 5$.

It is clear that the higher the number of cosine terms, the better the accuracy of the approximation. In order to simplify the discussion, the approximation of the sinc

function is done by using $R = 3$. Owing to this approximation, the simplified in-line hologram becomes

$$I(x) = \cos\left(\frac{\pi x^2}{\lambda z} - \frac{\pi}{4}\right)\left[\cos\left(\frac{2\pi f_0 x}{2}\right)\cos\left(\frac{2\pi f_0 x}{4}\right)\cos\left(\frac{2\pi f_0 x}{8}\right)\right]\text{rect}\left(\frac{x - L/2}{L}\right). \qquad (3.3)$$

By taking the property of the analytic function into account (see Appendix), the analytical expression of Eq. (3.3) can be written as

$$
\begin{aligned}
I_a(x) = \frac{1}{16}\Bigg\{ &\exp\left[j2\pi f_0\left(\frac{7}{8}x + \frac{\beta x^2}{2f_0} - \frac{1}{8f_0}\right)\right] + \exp\left[j2\pi f_0\left(-\frac{7}{8}x + \frac{\beta x^2}{2f_0} - \frac{1}{8f_0}\right)\right] \\
&+ \exp\left[j2\pi f_0\left(\frac{5}{8}x + \frac{\beta x^2}{2f_0} - \frac{1}{8f_0}\right)\right] + \exp\left[j2\pi f_0\left(-\frac{5}{8}x + \frac{\beta x^2}{2f_0} - \frac{1}{8f_0}\right)\right] \\
&+ \exp\left[j2\pi f_0\left(\frac{3}{8}x + \frac{\beta x^2}{2f_0} - \frac{1}{8f_0}\right)\right] + \exp\left[j2\pi f_0\left(-\frac{3}{8}x + \frac{\beta x^2}{2f_0} - \frac{1}{8f_0}\right)\right] \\
&+ \exp\left[j2\pi f_0\left(\frac{1}{8}x + \frac{\beta x^2}{2f_0} - \frac{1}{8f_0}\right)\right] + \exp\left[j2\pi f_0\left(-\frac{1}{8}x + \frac{\beta x^2}{2f_0} - \frac{1}{8f_0}\right)\right]\Bigg\} \\
&\times \text{rect}\left(\frac{x - L/2}{L}\right),
\end{aligned}
\qquad (3.4)
$$

where $\beta = 1/\lambda z$. The substitution of Eq. (3.4) into Eq. (2.5) gives the WVD output of fifteen components, which can be mathematically expressed as (see Appendix)

$$W_{Ia1}(x, f_x) = 2(L - 2|x - L/2|) \times \text{sinc}\{2(L - 2|x - L/2|) \times [f_x - f_0(7/8) - \beta x]\} \qquad (3.5.a)$$

$$
\begin{aligned}
W_{Ia2}(x, f_x) = &\{2\cos[2\pi f_0 x(2/8)]\} \times [2(L - 2|x - L/2|)] \\
&\times \text{sinc}\{2(L - 2|x - L/2|) \times [f_x - f_0(6/8) - \beta x]\}
\end{aligned}
\qquad (3.5.b)
$$

$$W_{Ia3}(x, f_x) = \{1 + 2\cos[2\pi f_0 x(4/8)]\} \times [2(L - 2|x - L/2|)]$$

$$\times \text{sinc}\{2(L - 2|x - L/2|) \times [f_x - f_0(5/8) - \beta x]\} \tag{3.5.c}$$

$$W_{Ia4}(x, f_x) = \{2\cos[2\pi f_0 x(6/8)] + 2\cos[2\pi f_0 x(2/8)]\} \times [2(L - 2|x - L/2|)]$$

$$\times \text{sinc}\{2(L - 2|x - L/2|) \times [f_x - f_0(4/8) - \beta x]\} \tag{3.5.d}$$

$$W_{Ia5}(x, f_x) = \{1 + 2\cos[2\pi f_0 x(8/8)] + 2\cos[2\pi f_0 x(4/8)]\}$$

$$\times [2(L - 2|x - L/2|)] \times \text{sinc}\{2(L - 2|x - L/2|) \times [f_x - f_0(3/8) - \beta x]\} \tag{3.5.e}$$

$$W_{Ia6}(x, f_x) = \{2\cos[2\pi f_0 x(10/8)] + 2\cos[2\pi f_0 x(6/8)] + 2\cos[2\pi f_0 x(2/8)]\}$$

$$\times [2(L - 2|x - L/2|)] \times \text{sinc}\{2(L - 2|x - L/2|) \times [f_x - f_0(2/8) - \beta x]\} \tag{3.5.f}$$

$$W_{Ia7}(x, f_x) = \{1 + 2\cos[2\pi f_0 x(12/8)] + 2\cos[2\pi f_0 x(8/8)] + 2\cos[2\pi f_0 x(4/8)]\}$$

$$\times [2(L - 2|x - L/2|)] \times \text{sinc}\{2(L - 2|x - L/2|) \times [f_x - f_0(1/8) - \beta x]\} \tag{3.5.g}$$

$$W_{Ia8}(x, f_x) = \{2\cos[2\pi f_0 x(14/8)] + 2\cos[2\pi f_0 x(10/8)] + 2\cos[2\pi f_0 x(6/8)]$$

$$+ 2\cos[2\pi f_0 x(2/8)]\} \times [2(L - 2|x - L/2|)]$$

$$\times \text{sinc}[2(L - 2|x - L/2|) \times (f_x - \beta x)] \tag{3.5.h}$$

$$W_{Ia9}(x, f_x) = \{1 + 2\cos[2\pi f_0 x(12/8)] + 2\cos[2\pi f_0 x(8/8)] + 2\cos[2\pi f_0 x(4/8)]\}$$

$$\times [2(L - 2|x - L/2|)] \times \text{sinc}\{2(L - 2|x - L/2|) \times [f_x + f_0(1/8) - \beta x]\} \tag{3.5.i}$$

$$W_{Ia10}(x, f_x) = \{2\cos[2\pi f_0 x(10/8)] + 2\cos[2\pi f_0 x(6/8)] + 2\cos[2\pi f_0 x(2/8)]\}$$

$$\times [2(L - 2|x - L/2|)] \times \text{sinc}\{2(L - 2|x - L/2|) \times [f_x + f_0(2/8) - \beta x]\} \quad (3.5.\text{j})$$

$$W_{Ia11}(x, f_x) = \{1 + 2\cos[2\pi f_0 x(8/8)] + 2\cos[2\pi f_0 x(4/8)]\}$$

$$\times 2(L - 2|x - L/2|) \times \text{sinc}\{2(L - 2|x - L/2|) \times [f_x + f_0(3/8) - \beta x]\} \quad (3.5.\text{k})$$

$$W_{Ia12}(x, f_x) = \{2\cos[2\pi f_0 x(6/8)] + 2\cos[2\pi f_0 x(2/8)]\}$$

$$\times [2(L - 2|x - L/2|)] \times \text{sinc}\{2(L - 2|x - L/2|) \times [f_x + f_0(4/8) - \beta x]\} \quad (3.5.\text{l})$$

$$W_{Ia13}(x, f_x) = \{1 + 2\cos[2\pi f_0 x(4/8)]\} \times [2(L - 2|x - L/2|)]$$

$$\times \text{sinc}\{2(L - 2|x - L/2|) \times [f_x + f_0(5/8) - \beta x]\} \quad (3.5.\text{m})$$

$$W_{Ia14}(x, f_x) = [2\cos(2\pi f_0 x(2/8))] \times [2(L - 2|x - L/2|)]$$

$$\times \text{sinc}\{2(L - 2|x - L/2|) \times [f_x + f_0(6/8) - \beta x]\} \quad (3.5.\text{n})$$

$$W_{Ia15}(x, f_x) = [2(L - 2|x - L/2|)] \times \text{sinc}\{2(L - 2|x - L/2|) \times [f_x + f_0(7/8) - \beta x]\}. \quad (3.5.\text{o})$$

The first and the fifteenth WVD components have similar expressions as shown in Eq. (2.9) in that they are equal to the product of the triangular and the two-dimensional (2-D) sinc functions. However, the spatial frequency of the sinc function is not only determined by $\beta = 1/\lambda z$, but also by the scaled f_0 (Widjaja and Chuamchaitrakool, 2013). The rests have their amplitudes modulated by a cosine,

triangular and sinc functions. Therefore, the WVD of the in-line hologram appears along a diagonal direction in the space spatial-frequency plane.

The summation of the fifteen WVD components can be expressed as Eq. (3.6), where m is the natural number of 1, 2, 3, ….

$$W_{I_a}(x, f_x) = \sum_{k=1}^{15}\left\{\sum_{m=1}^{k}(-1)^m + \sum_n 2\cos\left\{2\pi f_0\left[\frac{16 - 2(|8-n|+1)}{8}\right]x\right\}\right\}$$

$$\times 2\left(L - 2\left|x - \frac{L}{2}\right|\right) \times \mathrm{sinc}\left\{2\left(L - 2\left|x - \frac{L}{2}\right|\right) \times \left[f_x - \left(\frac{8-k}{8}\right)f_0 - \beta x\right]\right\}. \quad (3.6)$$

On the basis of this result, the general expression of the WVD of the simplified in-line hologram is given by

$$W_{I_a}(x, f_x) = \sum_{k=1}^{2^{R+1}-1}\left\{\sum_{m=1}^{k}(-1)^m + \sum_n 2\cos\left\{2\pi x f_0\left[\frac{2^{R+1} - 2(|2^R - n|+1)}{2^R}\right]\right\}\right\}$$

$$\times 2\left(L - 2\left|x - \frac{L}{2}\right|\right) \times \mathrm{sinc}\left\{2\left(L - 2\left|x - \frac{L}{2}\right|\right) \times \left[f_x - \left(\frac{2^R - k}{2^R}\right)f_0 - \beta x\right]\right\}, \quad (3.7)$$

where the number of the WVD components is equal to $2^{R+1}-1$. The conditions and index n in the summation of the cosine term in the above equation are expressed in Table 3.1, where l is any of the natural number of 1, 2, 3, … .

Table 3.1 Conditions for n in the summation of the cosine term in Eq. (3.7).

k	n
even and $\leq 2^{R+1}/2$	$2l \leq k$
even and $> 2^{R+1}/2$	$k+2(l\text{-}1) \leq 2^{R+1}-2$
odd and $\leq 2^{R+1}/2$	$2l\text{ -}1 \leq k$
odd and $> 2^{R+1}/2$	$k+2(l\text{-}1) \leq 2^{R+1}-1$

In order to verify the derivation, the WVD output from Eq. (3.6) is employed to compare with the one obtained from the in-line hologram generated by using Eq. (2.5). Figure 3.3 shows the top-view of WVDs calculated from Eq. (2.5) and Eq. (3.6), respectively.
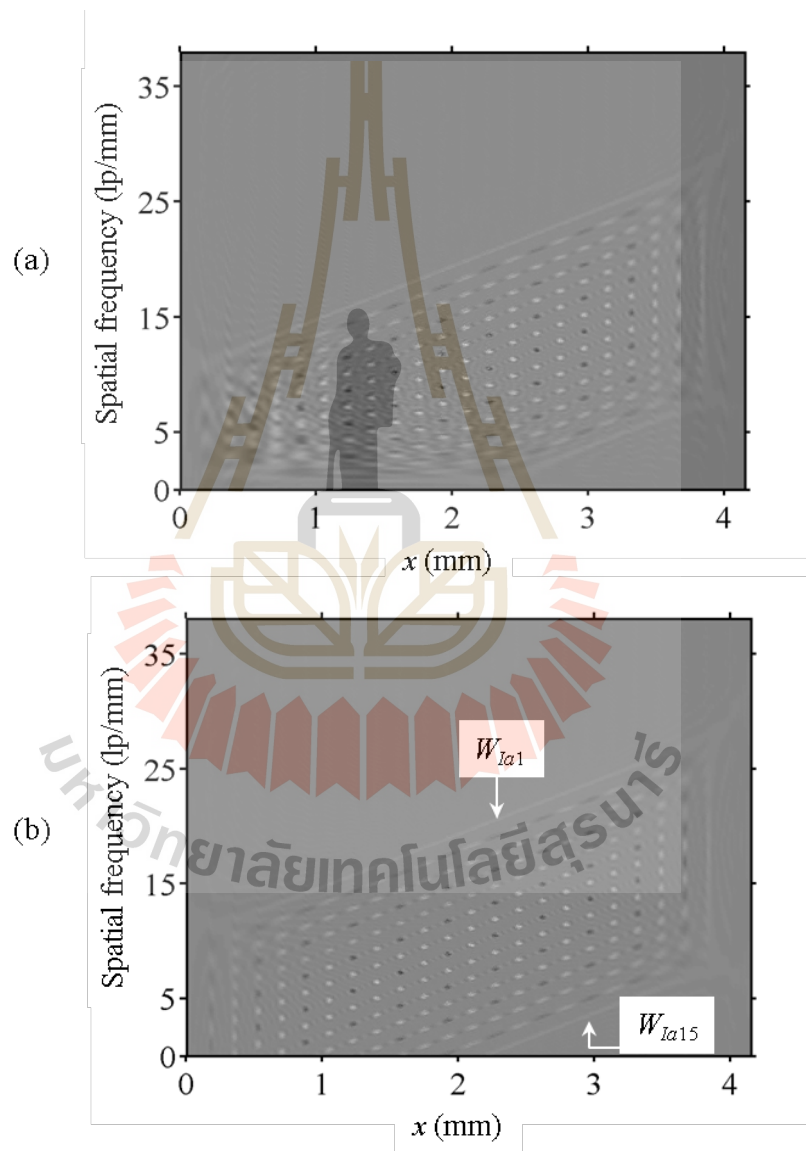
Figure 3.3 The WVD outputs calculated from (a) Eq. (2.5) and (b) Eq. (3.6) for the particle size $a = 2,500$ µm, respectively.

The comparison is done on the given parameters $z = 400$ mm, $\lambda = 543.5$ nm and $a = 2,500$ µm. It is noted that the bigger radius is employed to separate the 2-D sinc functions from each other due to it provides higher value of factor f_0. Figures 3.3(a) and 3.3(b) show the WVDs of Eq. (2.5) and Eq. (3.6), respectively.

In comparison with Figure 3.3(a), Figure 3.3(b) shows clearly that the fifteen components of the WVD appear along the same diagonal direction in the WVD plane. This verifies that they have the same frequency rate of change. The components of the WVD coefficients are now spread in the WVD plane, instead of being confined in the narrow area as shown in Figure 3.1. This is because the particle radius used in the generating of Figure 3.1 is approximately forty times smaller than that in Figure 3.3.

3.2   Particle Sizing by Using the WVD of In-Line Holograms

From the above fifteen WVD components in Eq. (3.5), the first and the last components can be utilized to extract the particle size. This is due to the fact that their mathematical expressions are simpler than the others. They can be further simplified into a single sinc function by considering them at a particular position $x = L/2$. At the particular position $x = L/2$, Eqs. (3.5.a) and (3.5.o) can be expressed as

$$W_{I_{a1}} = 2L\text{sinc}\left[2L\left(f_{x1} - \frac{7a}{8\lambda z} - \frac{L}{2\lambda z} \right) \right] \tag{3.8}$$

and

$$W_{I_{a15}} = 2L\text{sinc}\left[2L\left(f_{x2} + \frac{7a}{8\lambda z} - \frac{L}{2\lambda z} \right) \right]. \tag{3.9}$$

By taking the peak position of the sinc function into account, the peaks of W_{Ia1} and W_{Ia15} are located at

$$f_{x1} = \frac{7a}{8\lambda z} + \frac{L}{2\lambda z} \tag{3.10}$$

and

$$f_{x2} = \frac{-7a}{8\lambda z} + \frac{L}{2\lambda z}, \tag{3.11}$$

respectively. Therefore, scanning of the WVD output at the position $x = L/2$ along the spatial-frequency axis gives the two frequency peaks. The separation between the two peaks f_{x1} and f_{x2} can be expressed in terms of the number of pixels m in the spatial-frequency axis

$$m = \frac{(f_{x1} - f_{x2})}{\Delta f_x}, \tag{3.12}$$

where Δf_x is the spatial-frequency resolution of the WVD given by

$$\Delta f_x = (f_{CCD}/2)/N$$

$$= (N/2L)/N$$

$$= 1/2L, \tag{3.13}$$

where f_{CCD} is the frequency of the CCD image sensor. The substitutions of Eq. (3.10) and Eq. (3.11) into Eq. (3.12), yielding the particle size as

$$a = \left(\frac{4}{7}\right)\lambda z m \Delta f_x. \tag{3.14}$$

3.3 Flip and Replication Technique

In preceding section, the particle sizing method by using the WVD has been theoretically studied. However, the calculation of the particle size by using Eq. (3.14) shows that the accuracy of measurement is determined by the spatial-frequency resolution Δf_x. This equation implies that the accuracy of the particle size

measurement can become higher, provided that the size of the spatial-frequency resolution becomes finer.

Since the spatial-frequency resolution is inversely proportional to the length of the signal being analyzed, long hologram signals are required in order to improve the measurement accuracy. However, commercially available sensors generally have limited size, thus, the accuracy improvement can be accomplished by extending the length of hologram signals via flip and replication technique (FRT) (Chuamchaitrakool, Widjaja and Yoshimura, 2018). By applying the one- and the three-time FRTs to the original signal shown in Figure 2.4(b), the extended hologram signals whose lengths are one and three times longer than the original one can be obtained as shown in Figures 3.4(a) and (b), respectively.

In Figure 3.4(a), the one-time longer hologram is obtained by connecting the up-chirp signal of the original hologram with the down-chirp of the flipped hologram. Consequently, the extended holograms do not become discontinuous and a frequency artifact of the WVD can be minimized (Chuamchaitrakool, Widjaja and Yoshimura, 2015). For generating the three-time longer hologram signal shown in Figure 3.4(b), the FRT process is repeated three times. The discontinuity can now be avoided by connecting the down-chirp signal in Figure 3.4(a) with the up-chirp of its flipped hologram. Figures 3.4(c) and (d) are the WVD outputs corresponding to the extended hologram signals depicted in Figures 3.4(a) and (b), respectively. As a result of the length extensions, the spatial-frequency resolutions of the WVDs of the extended hologram signals shown in Figures 3.4(c) and (d) reduce to $1/4L$ and $1/8L$, respectively. Therefore, the three-time FRT has better spatial-frequency resolution than that of the one-time FRT.
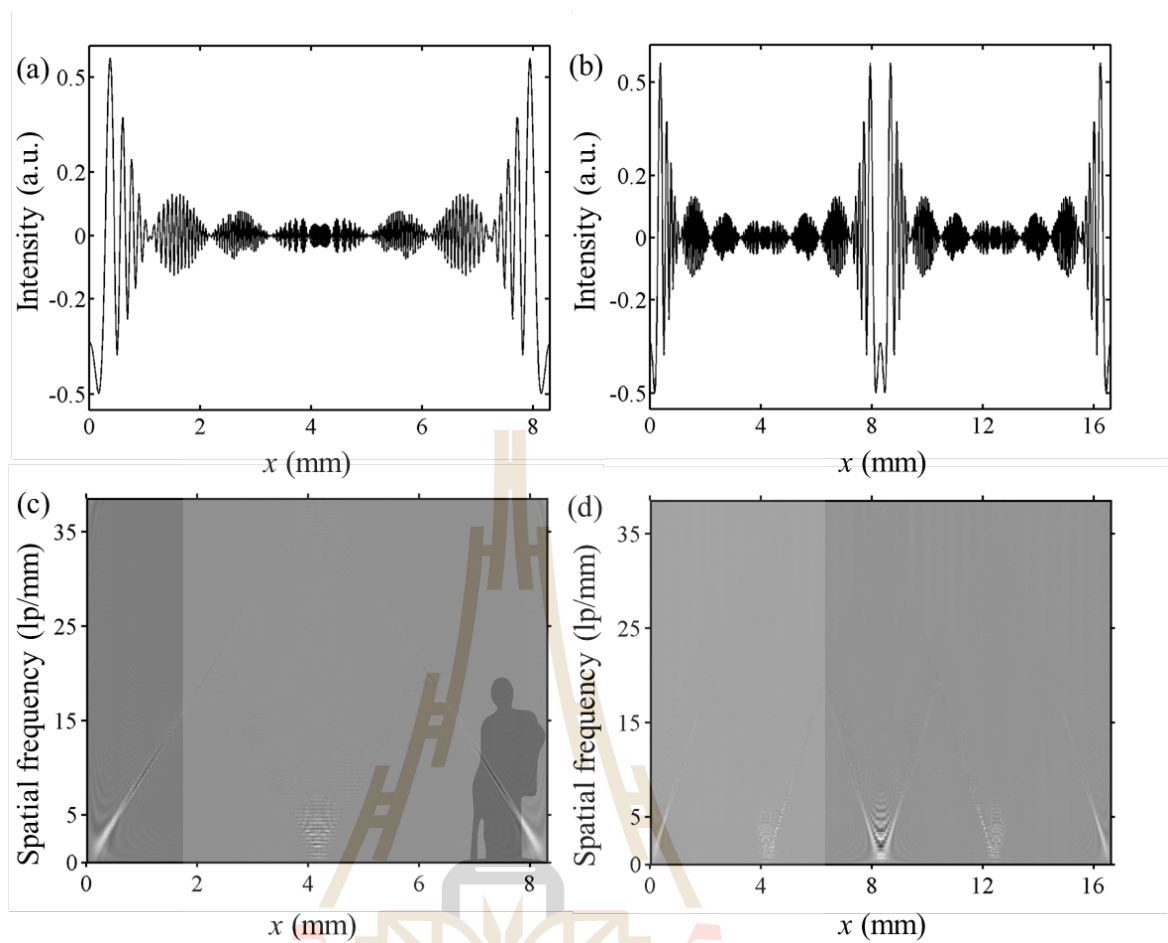
Figure 3.4 Extended signals obtained by applying the FRT (a) one and (b) three times

to the original hologram shown in Figure 2.4(b). The WVD outputs of the

extended signals shown in (c) Figure 3.4(a) and (d) Figure 3.4(b),

respectively.

In Figure 3.4(c), it is apparent that the WVD coefficients are now concentrated

along two diagonal directions with opposite-sign of slopes. The first concentrated

WVD output with positive slope describes the increase of the local frequency of the

up-chirp signal of the original hologram. While the second one with negative slope

corresponds to the down-chirp signal. Since the extended hologram contains two chirp

signals, frequency artifacts caused by an interference between their instantaneous

frequencies are generated in the midway $x = L$ between the two corresponding WVD coefficients. The reason that the artifacts are observable around low frequencies is that low-frequency components contain most signal energy. This interference is an inherent limitation of quadratic space-frequency signal representations (Kadambe and Boudreaux-Bartels, 1992). In Figure 3.4(d), the WVD output exhibits four concentrated WVD coefficients with the slopes alternate between positive and negative, because the original hologram was extended three times by the FRT. The existence of the frequency artifact can also be clearly observed from the figure. Owing to the proposed particle sizing method requires a scanning of signal along the spatial-frequency axis of the WVD output, therefore, it is important to study the interference effect on the proposed particle size measurement.

The interference effect was studied by comparing signals scanned along the spatial-frequency axis at $x = 2.075$ mm from the WVD outputs of the original and the extended holograms simulated at the recording distances $z = 200$ mm and 300 mm. The interference effect that is minimum, provided that the peaks f_{x1} and f_{x2} of the signals scanned from the WVD outputs of the extended holograms are identical to the original one. Figure 3.5 illustrates signals scanned along the spatial-frequency axis at $x = 2.075$ mm of the WVD outputs of the original and the extended hologram signals.

Figure 3.5(a) shows the 1-D scanned signals of the WVD outputs of the hologram recorded at the distance $z = 200$ mm, while Figure 3.6(b) is for that corresponds to the recording distance 300 mm. Since the WVDs of the extended holograms contain more coefficients, their scanned signals are accordingly down sampled to give the same number of pixels as that of the original hologram. The comparisons show that the desired peaks of the three scanned signals appear at the

same positions, regardless of the recording distances. This verifies that the frequency artifact occurred in the extended holograms does not degrade the signals scanned at the position $x = 2.075$ mm. Therefore, its effect on the particle size measurement is insignificant.
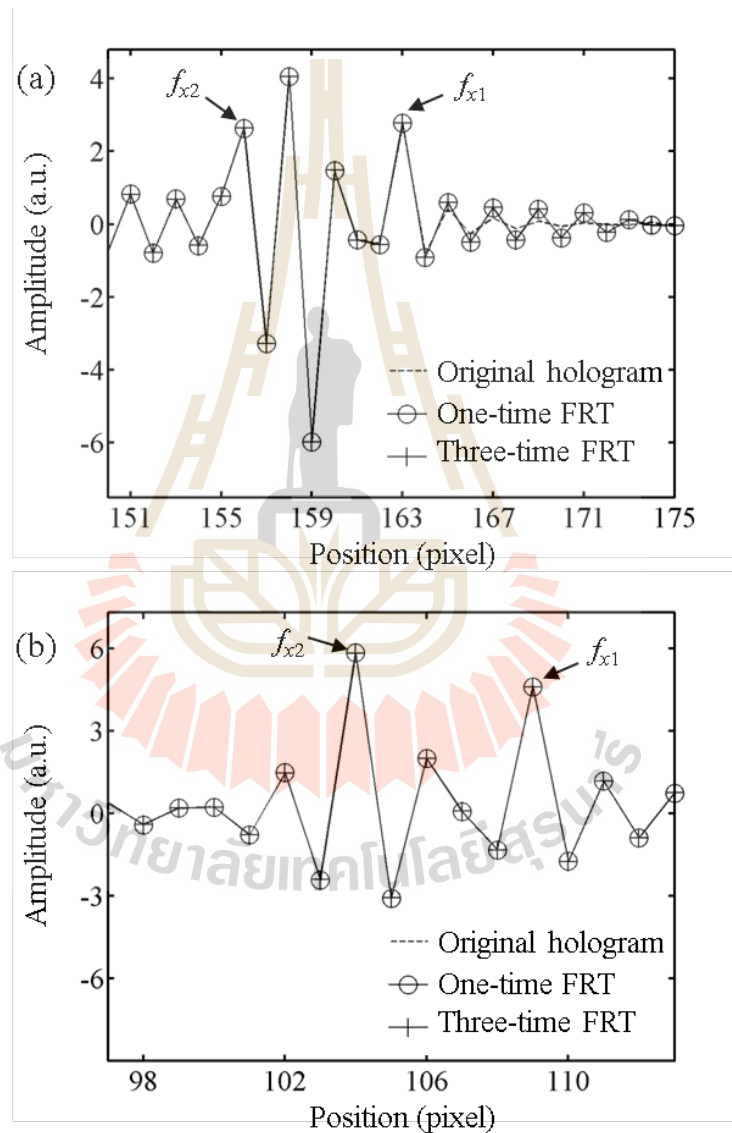
Figure 3.5 Signals scanned along the spatial-frequency axis at $x = 2.075$ mm of the WVD outputs of the original and the extended hologram signals with the recording distances (a) 200 mm and (b) 300 mm, respectively.

3.4   Measurement Performance

The preceding sections found that the WVD coefficients in the WVD plane encode information of the recording distance and the particle size. To analyze the measurement performance of the proposed particle sizing method, it is assumed that the hologram recording satisfies the Nyquist sampling theorem.

Figure 3.6 shows the distribution of the WVD coefficients of the hologram recorded at the minimum recording distance $z_{\min}$ in the WVD plane. Thus, the WVD output has the steepest slope.
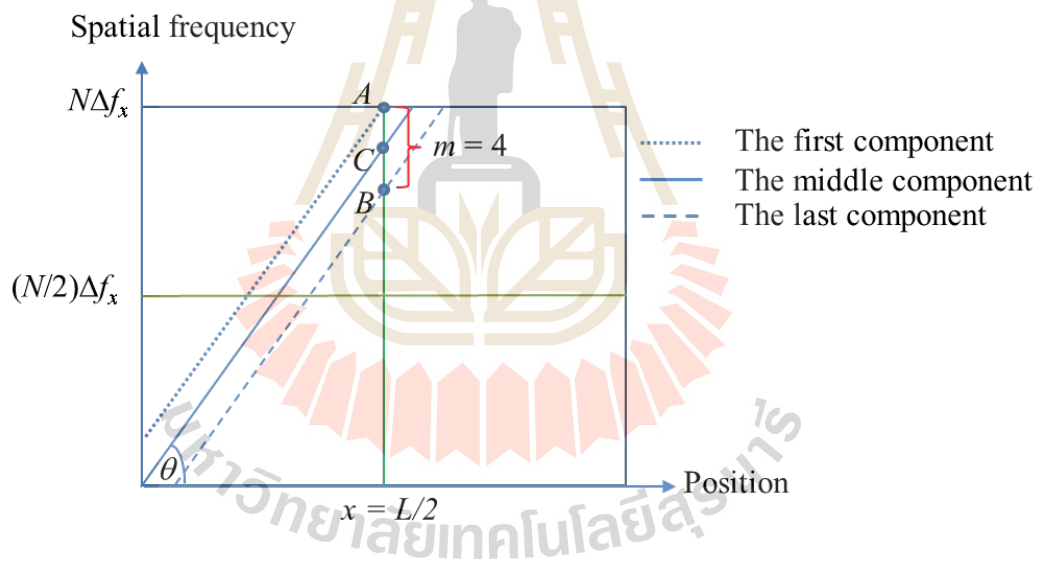
Figure 3.6 Distribution of WVD components of the hologram recorded at the minimum recording distance.

At position A, the value of the maximum spatial frequency is $N\Delta f_x$. The dot, the solid and the dash lines represent the first, the middle and the last WVD components. A, C and B represent the local spatial-frequencies of the first, the middle and the last WVD

components along the position $x = L/2$. In order to be able to measure the particle size, the local spatial-frequencies at the points A and B have to be resolvable at the steepest slope of the WVD output. In the case of the WVD output with fifteen components, the frequencies f_A and f_B are equal to f_{x1} and f_{x2}, respectively. The local spatial-frequency at point C is defined as f_C. In practice, the smallest separation of the two peaks f_{x1} and f_{x2} is $m_{min} = 4$. This value determines the minimum particle size that can be measured by the proposed method. Furthermore, this implies that the highest f_{x1} is equal to the maximum value of the spatial-frequency axis $N\Delta f_x$ and $f_{x2} = f_{x1} - 4\Delta f_x$. Since f_C belongs to the 8th WVD coefficient, Eq. (3.5.h) gives

$$f_C = \left(\frac{1}{\lambda z_{min}} \right) \frac{L}{2}. \tag{3.15}$$

Owing to position C is in the middle of positions A and B, the frequency at point C is also given by

$$f_C = \frac{f_{x1} + f_{x2}}{2}. \tag{3.16}$$

A substitution of Eq. (3.16) with $f_{x1} = N\Delta f_x$ and $f_{x2} = f_{x1} - 4\Delta f_x$ gives

$$f_C = \frac{N\Delta f_x + (N-4)\Delta f_x}{2} = \frac{N-2}{2L}. \tag{3.17}$$

The substitution of Eq. (3.17) into Eq. (3.15) gives the shortest recording distance z_{min} as

$$z_{min} = \frac{L^2}{\lambda(N-2)}. \tag{3.18}$$

The smallest particle size that can be measured at the distance z_{min} is obtained by substituting Eq. (3.18) into Eq. (3.14)

$$a_{\min @ z_{\min}} = \frac{8L}{7(N-2)}. \tag{3.19}$$

Figure 3.7 shows the distribution of the WVD output of the hologram recorded at the maximum recording distance $z_{\max}$. The maximum recording distance causes the mildest slope of the WVD output with $f_{x2} = \Delta f_x$. By keeping the resolvable separation between f_{x1} and f_{x2} is $m = 4$, f_{x1} is equal to $5\Delta f_x$. Thus,

$$f_C = \frac{5\Delta f_x + \Delta f_x}{2} = \frac{3}{2L}. \tag{3.20}$$
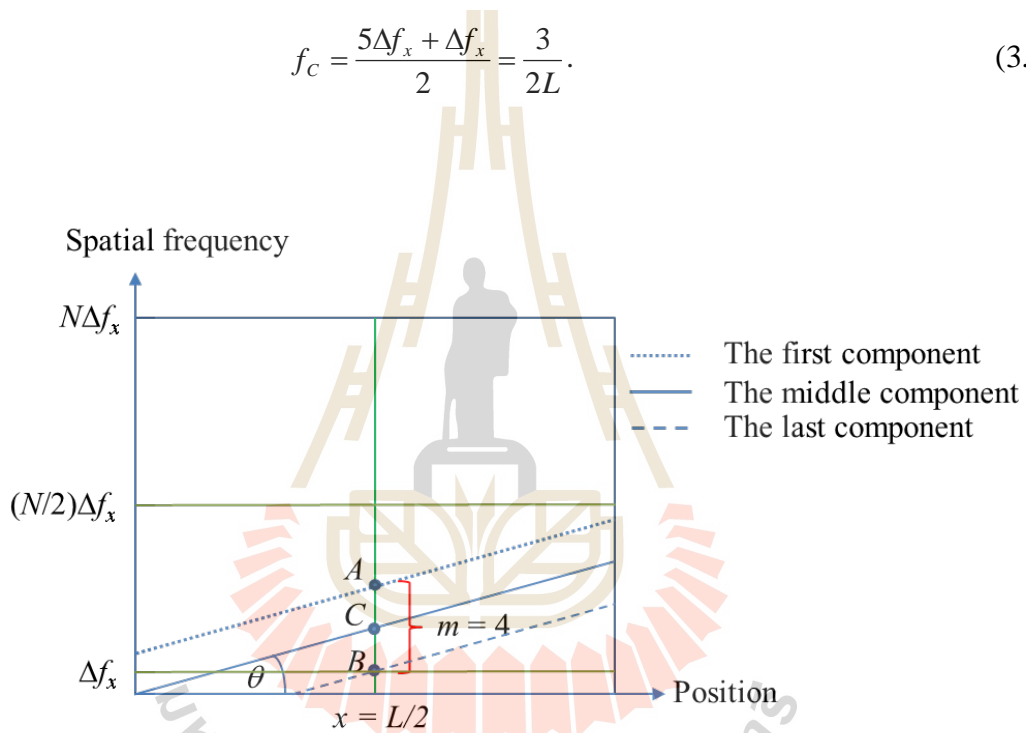
Figure 3.7 Distribution of WVD components of the hologram recorded at the maximum recording distance.

In Figure 3.7, the frequency at point C is inverse proportional to the maximum recording distance $z_{\max}$ as

$$f_C = \left(\frac{1}{\lambda z_{\max}}\right)\frac{L}{2}. \tag{3.21}$$

A substitution of Eq. (3.20) into Eq. (3.21) gives

$$z_{\max} = \frac{L^2}{3\lambda}. \tag{3.22}$$

The minimum measurable particle size at the distance $z_{\max}$ is obtained by substituting Eq. (3.22) into Eq. (3.14)

$$a_{\min@z_{\max}} = \frac{8L}{21}. \tag{3.23}$$

Figure 3.8 shows the distribution of the WVD output of the hologram recorded at the critical recording distance z_{critical}.
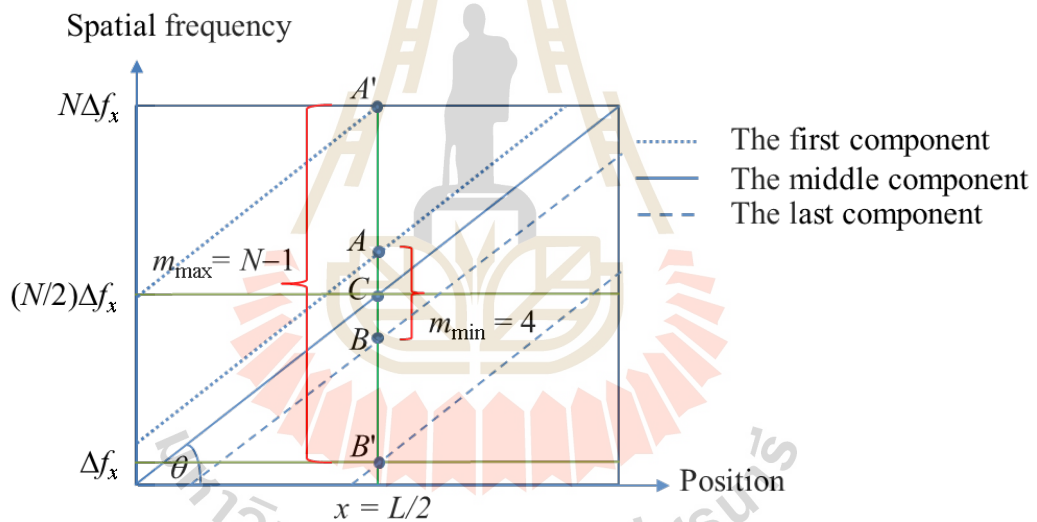
Figure 3.8 Distribution of WVD components of the hologram recorded at the critical recording distance.

Owing to the property of the proposed method, the maximum particle size that can be measured corresponds to the highest separation $m\Delta f_x$ between the peaks at frequencies f_{x1} and f_{x2}. This separation condition is achieved when the peaks appear at

$f_{x1} = (N-1)\Delta f_x$ and $f_{x2} = \Delta f_x$ or $m_{max} = N-2$. Consequently, the frequency f_C is determined as

$$f_C = \frac{f_{x1} + f_{x2}}{2} = \frac{N}{4L}. \tag{3.24}$$

In Figure 3.8, the frequency at point C is inverse proportional to the maximum recording distance z_{max} as

$$f_C = \left(\frac{1}{\lambda z_{\text{critical}}} \right) \frac{L}{2}. \tag{3.25}$$

A substitution of Eq. (3.24) into Eq. (3.25) gives a critical recording distance that allows the measurement of the largest particle

$$z_{\text{critical}} = \frac{2L^2}{\lambda N}. \tag{3.26}$$

Thus, the largest measurable particle size can be determined by substituting m_{max} and z_{critical} into Eq. (3.14)

$$a_{\max @ z_{\text{critical}}} = \frac{4L}{7} \left(\frac{N-2}{N} \right). \tag{3.27}$$

It is worth mentioning that by taking $m_{min} = 4$ into account, it is possible to measure the minimum particle size at the distance z_{critical}

$$a_{\min @ z_{\text{critical}}} = \frac{16L}{7N}. \tag{3.28}$$

CHAPTER IV

EXPERIMENTAL VERIFICATIONS

This chapter discusses the experimental verifications of the proposed particle sizing method by using the WVD and the improvement of its measurement accuracy by using the FRT. Firstly, the experimental and the simulation results from the in-line particle holograms are described. Secondly, the particle sizing from the hologram signals extended by using the FRT is compared with that from the original holograms.

4.1 Experimental Verifications of the WVD-based Particle Sizing

Feasibility of the proposed particle sizing method was verified through the computer simulations and the experiments. The holograms were experimentally generated by using the setup shown in Figure 4.1. In the setup, a coherent light generated from a He-Ne laser source (Melles Griot, 05-LGR-193, USA) with the operating wavelength $\lambda = 543.5$ nm was collimated by using a spatial filter and a collimating lens. An optical fiber having a diameter of 124.96 µm was used as the test object. Its interference patterns were recorded by a CCD image sensor (Hamamatsu C5948) with resolution of 640×480 pixels in the area of 8.30×6.30 mm². The recording distances z were varied from 200 mm to 400 mm by an interval of 100 mm. The length of the holograms being analyzed was $L = 4.15$ mm consisting of 320 pixels.
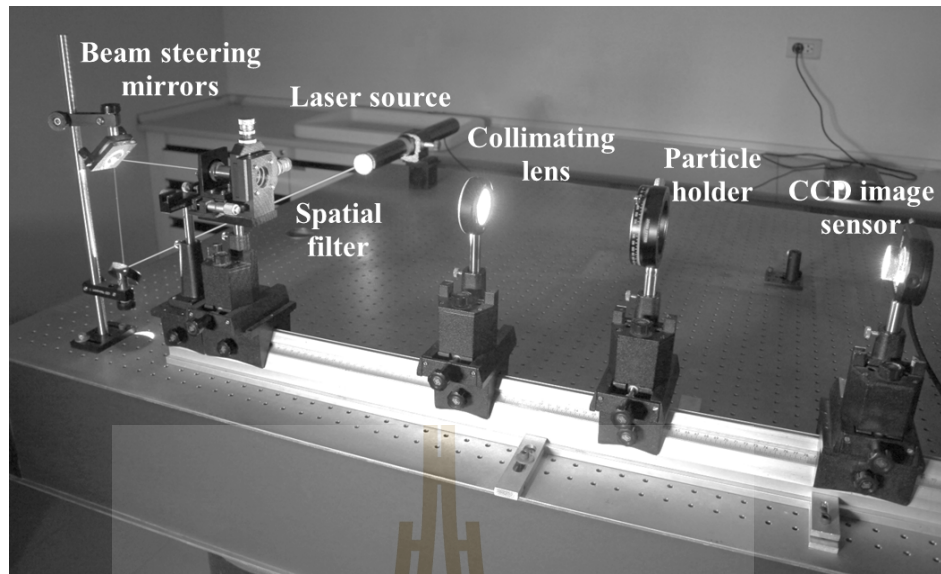
Figure 4.1 Experimental setup for generating in-line holograms.

Figure 4.2 shows the intensity transmittances of the simulated and the experimentally generated in-line holograms of the optical fiber with a dc removal at the recording distance $z = 400$ mm. They are represented by the broken and the solid lines, respectively. Their analytic representations were generated by using the Hilbert transform function of MATLAB. After calculating the WVD of the holograms by using Eq. (2.5), the output WVD coefficients were employed for extracting the particle sizes.

In order to obtain the acceptable accuracy of the measurement, the WVD of a product of five cosine functions was employed for the sinc approximation. Thus, the first and the sixty-third components obtained from Eq. (3.7) can be expressed as

$$W_{Ia1}(x, f_x) = 2\left(L - 2\left|x - \frac{L}{2}\right|\right) \times \mathrm{sinc}\left\{2\left(L - 2\left|x - \frac{L}{2}\right|\right) \times \left[f_x - f_0\left(\frac{31}{32}\right) - \beta x\right]\right\} \qquad (4.1)$$

and

$$W_{Ia63}(x, f_x) = 2\left(L - 2\left|x - \frac{L}{2}\right|\right) \times \mathrm{sinc}\left\{2\left(L - 2\left|x - \frac{L}{2}\right|\right) \times \left[f_x + f_0\left(\frac{31}{32}\right) - \beta x\right]\right\}, \qquad (4.2)$$

respectively.
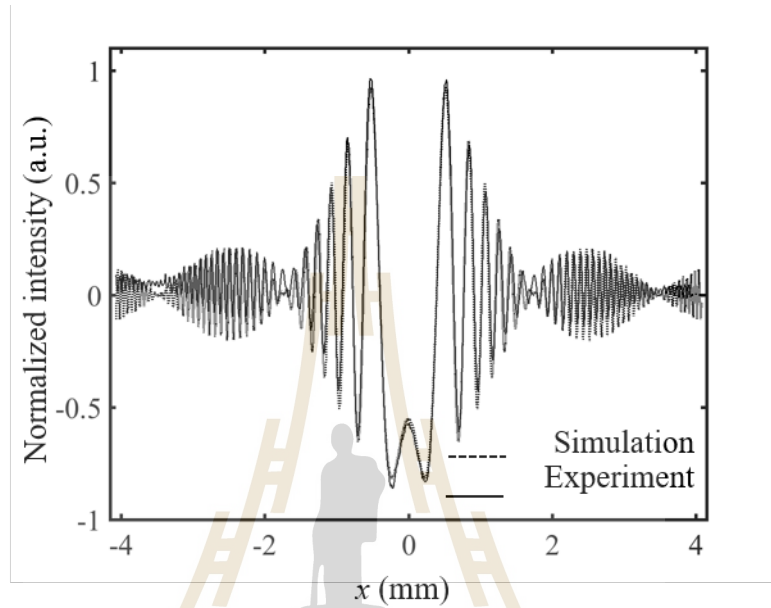
Figure 4.2 Normalized intensity transmittances of the simulated and the experimentally generated in-line holograms of the optical fiber with a diameter of 124.96 µm at the distance $z = 400$ mm.

At the particular position $x = L/2$, Eqs. (4.1) and (4.2) can be expressed as

$$W_{I_{a1}} = 2L\mathrm{sinc}\left[2L\left(f_{x1} - \frac{31a}{32\lambda z} - \frac{L}{2\lambda z}\right)\right] \qquad (4.3)$$

and

$$W_{I_{a63}} = 2L\mathrm{sinc}\left[2L\left(f_{x2} + \frac{31a}{32\lambda z} - \frac{L}{2\lambda z}\right)\right]. \qquad (4.4)$$

Therefore, the peaks of the both sinc functions are located at

$$f_{x1} = \frac{31a}{32\lambda z} + \frac{L}{2\lambda z} \qquad (4.5)$$

and

$$f_{x2} = \frac{-31a}{32\lambda z} + \frac{L}{2\lambda z},$$ (4.6)

respectively. Finally, the substitutions of Eqs. (4.5) and (4.6) into Eq. (3.12) give the particle size as

$$a = \left(\frac{16}{31}\right)\lambda z m \Delta f_x.$$ (4.7)

Owing to the sixty-third WVD components, the measurement performance at z_{min} and z_{max} can be re-expressed as

$$a_{min@\, z_{min}} = \frac{32L}{31(N-2)}$$ (4.8)

and

$$a_{min@\, z_{max}} = \frac{32L}{93}.$$ (4.9)

While a_{min} and a_{max} at $z_{critical}$ are given by

$$a_{min@\, z_{critical}} = \frac{64L}{31N}$$ (4.10)

and

$$a_{max@\, z_{critical}} = \frac{16L}{31}\left(\frac{N-2}{N}\right).$$ (4.11)

Performance of the proposed particle sizing from the hologram recorded for given parameters $\lambda = 543.5$ nm, $L = 4.15$ mm and $N = 320$ pixels is depicted in Table 4.1. It is obvious that the particle sizing performance depends mainly on the resolution of the array sensors. Figure 4.3 shows a plot of tetragonal shape representing the measurable particle sizes corresponding to the recording distances.

Although there are three minimum particle sizes that can be measured by the proposed method, $a_{\text{min@zmin}}$ shown in Figure 4.3 is the smallest size.

Table 4.1 Performance of the proposed particle sizing from the holograms recorded for given parameters $\lambda = 543.5$ nm, $L = 4.15$ mm and $N = 320$ pixels.

	$z_{\text{min}} = \dfrac{L^2}{\lambda(N-2)}$	$z_{\text{max}} = \dfrac{L^2}{3\lambda}$	$z_{\text{critical}} = \dfrac{2L^2}{\lambda N}$
	$= 99.65$ mm	$= 10{,}562.71$ mm	$= 198.05$ mm
a_{min}	$\dfrac{32L}{31(N-2)} = 13.47$ μm	$\dfrac{32L}{93} = 1{,}427.96$ μm	$\dfrac{64L}{31N} = 26.77$ μm
a_{max}	-	-	$\dfrac{16L}{31}\left(\dfrac{N-2}{N}\right) = 2{,}128.55$ μm

Figure 4.3 Performance of measurable particle size as a function of the recording distance.

In order to verify the measurement performance shown in Table 4.1, three holograms of the original sinc function were simulated by using Eq. (2.4) at the

corresponding recording distances and particle sizes. Figures 4.4(a) and (b) show the WVDs of the holograms at the particle sizes 13.47 µm and 1,427.96 µm, respectively. The holograms were simulated at the minimum and the maximum recording distances $z_{min} = 99.65$ mm and $z_{max} = 10,562.71$ mm.

In comparison with Figure 4.4(b), the slope of the WVD output in Figure 4.4(a) is higher, because its recording distance is shorter. Since both holograms record the particles with the minimum sizes, their WVD coefficients are concentrated along the diagonal direction. Their corresponding WVD coefficients scanned along the spatial-frequency axis at $x = L/2$ are depicted in Figures 4.4(c) and (d), respectively. It is apparent that the two frequency peaks f_{x1} and f_{x2} are clearly separated.

In the case of the holograms of the particle with the minimum and the maximum sizes recorded at the critical recording distance, the analyses by using the WVD gave the outputs shown in Figures 4.5(a) and (b), respectively. The significant coefficients of the WVD output in Figure 4.5(a) concentrate in the narrow area, while those in Figure 4.5(b) spread in the WVD plane. Thus, the separation of the two frequency peaks, f_{x1} and f_{x2}, in Figure 4.5(a) is narrower than that in Figure 4.5(b). In summary, the results verify the analysis of the sizing performance of the proposed method.
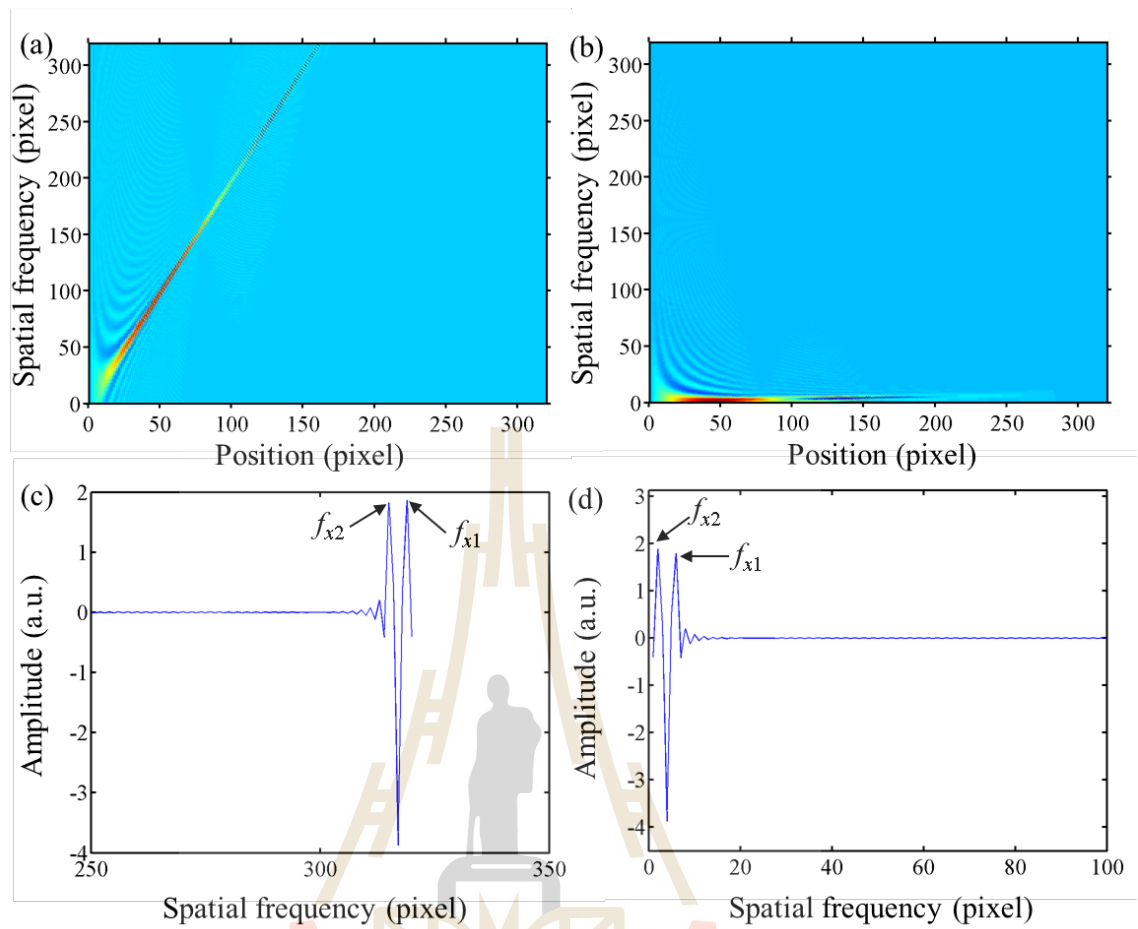
Figure 4.4 WVD outputs of the in-line holograms of the particles with minimum sizes (a) $a = 13.47$ μm recorded at $z_{min} = 99.65$ mm and (b) $a = 1,427.96$ μm recorded at $z_{max} = 10,562.71$ mm. The corresponding WVD coefficients of (c) Figure 4.4(a) and (d) Figure 4.4(b) scanned along the spatial frequency at $x = L/2$, respectively.
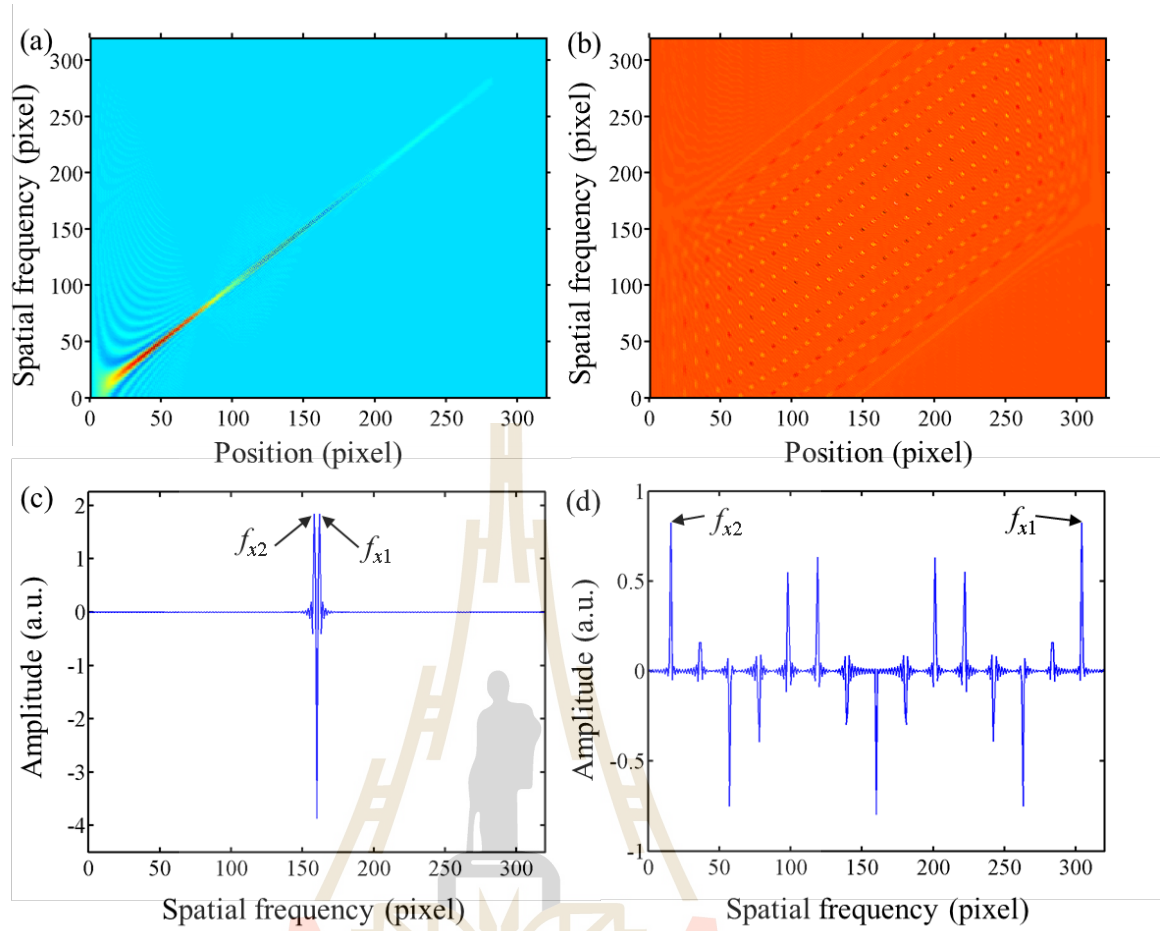
Figure 4.5 WVD outputs of the in-line holograms of the particles with the minimum size (a) a = 26.77 µm and (b) the maximum size a = 2,128.55 µm recorded at $z_{critical}$ = 198.05 mm. The corresponding WVD coefficients of (c) Figure 4.5(a) and (d) Figure 4.5(b) scanned along the spatial frequency at x = $L/2$, respectively.

Figure 4.6 shows the WVD coefficients scanned from the WVDs of the simulated and the experimentally generated holograms of the optical fiber at x = 2.075 mm along the spatial-frequency axis. They are compared with the WVD components W_{Ia1} and W_{Ia63} given by using Eq. (4.1) and Eq. (4.2), respectively. The plots show obviously that the maximum peaks of W_{Ia1} and W_{Ia63} overlap with those obtained

from the WVDs of the simulated and the experimentally generated holograms. By determining the number of pixels m between the peaks W_{Ia1} and W_{Ia63}, the particle size can be calculated by using Eq. (4.7).
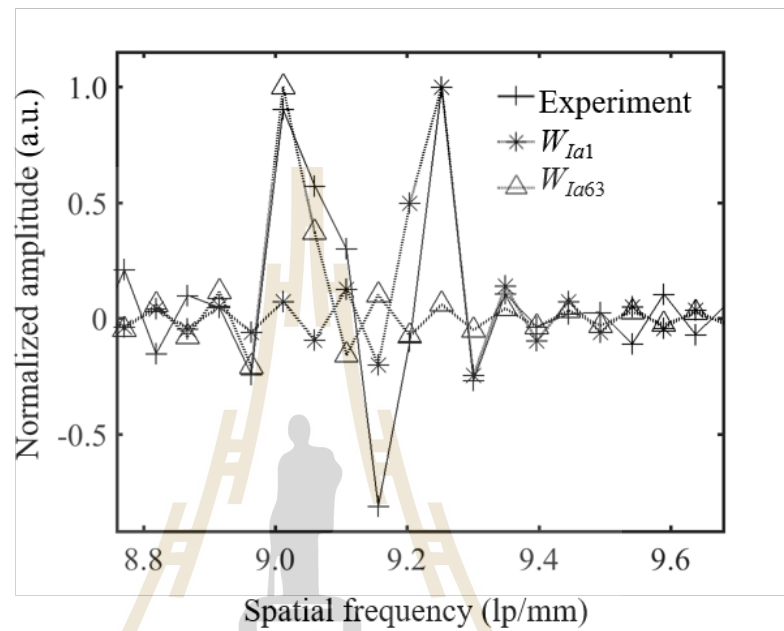
Figure 4.6 A comparison of the coefficients scanned at $x = L/2$ along the spatial-frequency axis from the WVDs of the experimentally generated hologram compared with the WVD components of $W_{I_{a}1}$ and $W_{I_{a}63}$.

Table 4.2 shows the errors in the particle size measurements from the simulated and the experimentally generated holograms recorded at the distances 200, 300 and 400 mm by using the proposed particle sizing method. Unlike the case of the simulated holograms, the experiment has higher errors for the short recording distance. This may be caused by the fact that speckle noise inherently occurring in the experiment degrades the recorded holograms. Moreover, the undersampling effect is

stronger for the short recording distance, and the amplitude of the second term of Eq. (2.4) increases as the recording distance becomes shorter. The amplitudes of the 2nd and the 3rd terms in Eq. (2.4) are determined by the factors $4a^2/\lambda z$ and $4a/(\lambda z)^{0.5}$, respectively. Their values and ratios for different distances shown in Table 4.3 reveal that as the recording distance is shorter, the maximum amplitude of the 2nd term increases. For this reason, the second term could be presented as a noise in the hologram signal recorded at a shorter recording distance. Consequently, the WVD of the corresponding hologram will differ from the WVD of the simplified hologram. Therefore, the measurement errors become higher.

Table 4.2 Errors in the size measurement of the optical fiber by using the WVD.

Recording distance z (mm)	Measurement errors (%)	
	Simulated in-line holograms	Experimentally generated in-line holograms
200	4.508	5.409
300	1.078	1.078
400	0.9044	0.9044

Table 4.3 The amplitudes of the 2nd and the 3rd terms in Eq. (2.4).

	$a = 50 \, \mu m$	
	$z = 20$ cm	$z = 30$ cm
Max of 2nd term	0.09200	0.06130
Max of 3rd term	0.6066	0.4953
Ratio of 2nd to 3rd terms	0.1517	0.1238

4.2 Experimental Verifications of the FRT

The verifications of the FRT were done by experimental generating the holograms of a polycarbonate microtube with a diameter of 100 µm (Paradigm Optics, Inc., USA). The microtube was placed along the vertical direction in front of the same CCD sensor used in the setup shown in Figure 4.1. The recording distances were varied from 200 mm to 300 mm with an interval of 20 mm. The hologram signals along the positive axis x with the length L of 4.15 mm and consisted of 320 pixels were used as the original holograms. One- and three-time FRTs were then applied to the original holograms. After removing the dc signals, Hilbert transform function of MATLAB was used to generate their analytic functions. The WVDs of the simulated and the experimentally generated holograms were computed, yielding the spatial-frequency resolutions of 120.4, 60.20 and 30.10 lp/m for the original, the one-time and the three-time extended holograms, respectively. The same particle sizing was calculated by using Eq. (4.7).

Table 4.4 shows a comparison of the errors in the size measurements of the polycarbonate microtube from the simulated and the experimentally generated

holograms with and without FRTs. The results show that firstly, the measurement errors from both types of holograms reduce as the recording distance becomes longer, regardless of the hologram lengths. This is due to the fact that at the shorter recording distance, the cosine chirp signal has higher frequency.

Figure 4.7 shows plots of the two hologram signals obtained from the experiments after the dc background removal at the recording distances $z = 200$ mm and $z = 220$ mm. In Figure 4.7(a), it can be observed that the signal suffers from the undersampling effect starting around $x = 2.080$ mm. For Figure 4.7(b), the undersampling effect starts after $x = 2.350$ mm. For this reason, the WVD coefficients obtained from the hologram recorded at the distance $z = 200$ mm gives higher measurement errors than those from the longer recording distances. Thus, an effect of undersampling on the hologram recordings is more significant.

Secondly, the measurement errors for all recording distances decrease by using the three-time FRT. This is understandable since the three-time FRT reduces the spatial-frequency resolution of the WVD outputs more than the others. Finally, the measurement errors from the experimentally generated in-line holograms appear slightly higher than those of the simulated holograms, because speckle noise is inherently present in the experiment.

Table 4.4 Errors in the size measurement of the polycarbonate microtube by using the WVDs of the simulated and the experimentally generated holograms.

Recording distance z (mm)	Measurement errors (%)					
	Simulated in-line holograms			Experimentally generated in-line holograms		
	Without FRT	One-time FRT	Three-time FRT	Without FRT	One-time FRT	Three-time FRT
200.0	5.432	4.307	2.167	8.077	4.700	2.167
220.0	4.024	2.167	1.548	4.024	3.406	1.548
240.0	2.730	1.322	1.322	2.730	2.673	1.322
260.0	2.448	0.9847	0.9847	2.448	1.942	1.211
280.0	2.280	0.7040	0.7040	2.280	0.7040	0.7040
300.0	1.322	0.3663	0.3663	1.322	0.3663	0.3663
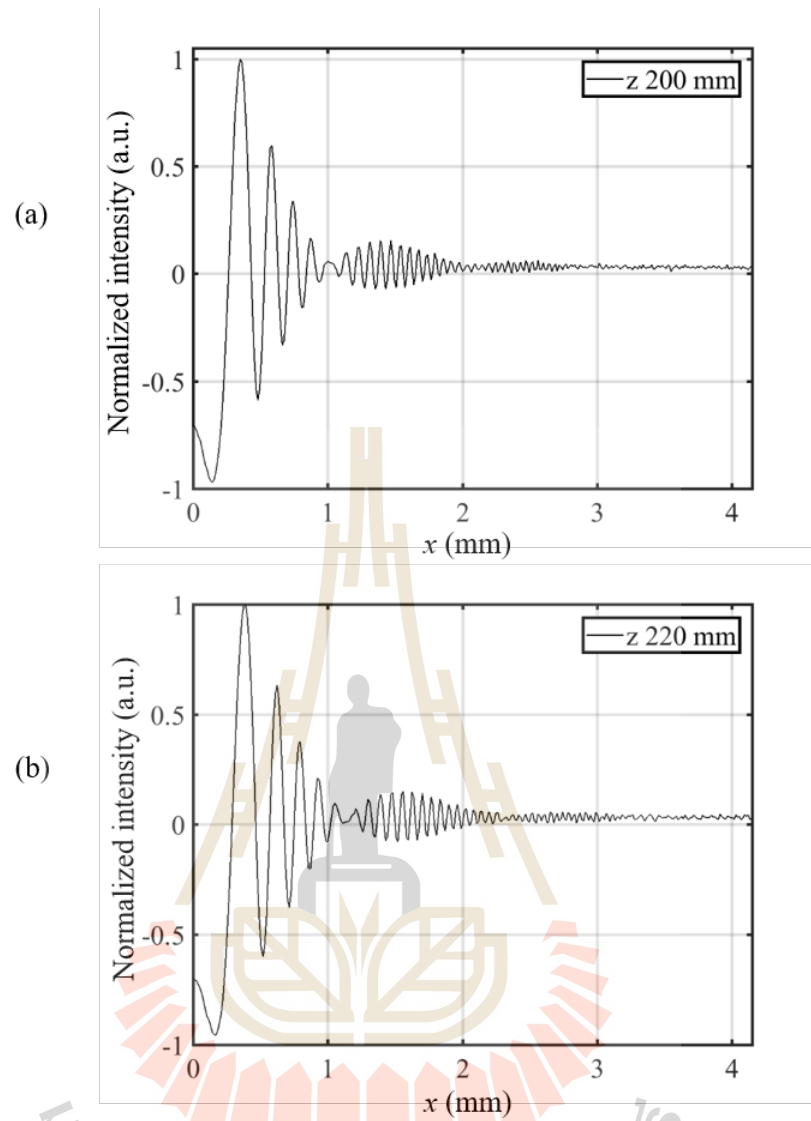
Figure 4.7 Hologram signals from the experiment generated at the recording
distances (a) z = 200 mm and (b) z = 220 mm.

CHAPTER V

CONCLUSIONS

This thesis has proposed and verified experimentally a new method for extracting the size of an object with high aspect ratio from an in-line hologram by using the WVD. The proposed method is based on the mathematical derivation of the WVD of the in-line hologram. The derivation result shows that the size of the object being studied can be obtained from the local frequencies scanned at the half length of the hologram being analyzed. The proposed method has advantages over the conventional numerical reconstruction in that first, it is free from iterative processes. Secondly, the method can extract the object size and its position by using a single computation of the WVD. Thirdly, the conventional numerical reconstruction methods measure the particle size from the reconstructed images. Therefore, the sizing accuracy depends on the spatial resolution of the image sensor. In order to have high sizing accuracy, the conventional methods require a sensor with high spatial resolution. In contrast, the WVD performs the particle sizing in the spatial-frequency domain. Consequently, the sizing accuracy is determined by the spatial-frequency resolution Δf_x. In this thesis, the method for improving the measurement accuracy by using the FRT has also been studied.

The theoretical analysis of the particle sizing method shows that the accuracy of the calculated particle size is dependent upon the spatial-frequency resolution of the WVD. In order to improve the accuracy of the particle size measurement via the

proposed method, the FRT has been proposed and experimentally verified. By the flip and the replication processes, the hologram length can be extended without discontinuity. The experimental results verify that although the frequency artifact caused by the signal extension occurs in the WVD plane, its effect on the size measurement is minimum. Therefore, the accuracy in the particle size measurements can be improved by using the proposed FRT. The proposed method is suitable for particle sizing from holograms recorded by using small size image sensors.

REFERENCES

REFERENCES

Black, D. L., McQuay, M. Q. and Bonin, M. P. (1996). Laser-based techniques for particle size measurement: A review of sizing methods and their industrial applications. **Prog. Energy Combust. Sci.** 22: 267-306.

Boashash, B. (1988). Note on the use of the Wigner distribution for time-frequency analysis. **IEEE Trans. Acoust. Speech Signal Proc.** 36: 1518-1521.

Buraga-Lefebvre, C., Coëtmellec, S., Lebrun, D. and Özkul, C. (2000). Application of wavelet transform to hologram analysis: three-dimensional location of particles. **Opt. Lasers Eng.** 33: 409-421.

Carl, D., Kemper, B., Wernicke, G. and Von Bally, G. (2004). Parameter-optimized digital holographic microscope for high-resolution living-cell analysis. **Appl. Opt.** 43(36): 6536-6544.

Choi, Y-K. and Lee, S-J. (2009). Three-dimensional volumetric measurement of red blood cell motion using digital holographic microscopy. **Appl. Opt.** 48: 2983-2990.

Chuamchaitrakool, P., Widjaja, J. and Yoshimura, H. (2015). Holographic particle sizing using Wigner-Ville distribution. **Opt. Lasers Eng.** 67: 186-190.

Chuamchaitrakool, P., Widjaja, J. and Yoshimura, H. (2018). Improved accuracy in Wigner-Ville distribution-based sizing of rod-shaped particle by using flip and replication technique," **Opt. Eng.** 57(1): 014105.

Darakis, E., Khanam, T., Rajendran, A., Kariwala, V., Naughton, T. J. and Asundi, A. K. (2010). Microparticle characterization using digital holography. **Chem. Eng. Sci.** 65(2): 1037-1044.

Ferrara, M. A., Angelis, A. D., Luca, A. C. D., Coppola, G., Dale, B. and Coppola, G. (2016). Simultaneous holographic microscopy and Raman spectroscopy monitoring of human spermatozoa photodegradation. **IEEE J. Sel. Topics Quantum Electron.** 22(3): 27-34.

Goodman, J. W. (1996). **Introduction to Fourier Optics.** 2nd ed., Singapore: McGraw-Hill.

Guildenbecher, D. R., Cooper, M. A., Gill, W., Stauffacher, H. L., Oliver, M. S. and Grasser, T. W. (2014). Quantitative, three-dimensional imaging of aluminum drop combustion in solid propellant plumes via digital in-line holography. **Opt. Lett.** 39: 5126-5129.

Hariharan, P. (1996). **Optical Holography: Principle, Techniques, and Applications.** Cambridge: University Press.

Hlawatsch, F. Interference terms in the Wigner distribution. In: Cappellini V, Constantinidies A. G., editors. **Digital Signal Processing.** North-Holland: Elsevier: 1984. p. 363-367.

Javidi, B., Moon, I., Yeom, S. and Carapezza, E. (2005). Three-dimensional imaging and recognition of microorganism using single-exposure on-line (SEOL) digital holography. **Opt. Exp.** 13(12): 4492-4506.

Kadambe, S. and Boudreaux-Bartels, G. F. (1992). A comparison of the existence of `cross terms' in the Wigner distribution and the squared magnitude of the wavelet

transform and the short-time Fourier transform. **IEEE Trans. Signal Processing.** 40(10): 2498-2517.

Kemper, B., Barroso, Á., Woerdemann, M., Dewenter, L., Vollmer, A., Schubert, R., Mellmann, A., Von Bally, G. and Denz, C. (2013). Towards 3D modeling and imaging of infection scenarios at the single cell level using holographic optical tweezers and digital holographic microscopy. **J. Biophotonics.** 6(3): 260-266.

Khanam, T., Rahman, M. N., Rajendran, A., Kariwala, V. and Asundi, A. K. (2011). Accurate size measurement of needle-shaped particles using digital holography. **Chem. Eng. Sci.** 66: 2699-2706.

Kim, S. and Lee, S. J. (2007). Measurement of 3D larminar flow inside a micro tube using micro digital holographic particle tracking velocimetry. **J. Micromech. Microeng.** 17: 2157-2162.

Langehanenberg, P., Kemper, B., Dirksen, D. and Bally, G. V. (2008). Autofocusing in digital holographic phase contrast microscopy on pure phase objects for live cell imaging. **Appl. Opt.** 47: D176-D182.

Lee, S. J., Seo, K. W., Choi, Y. S. and Sohn, M. H. (2011). Three-dimensional motion measurements of free-swimming microorganisms using digital holographic microscopy. **Meas. Sci. Technol.** 22(6): 4004-4011.

Mallahi, E., Minetti C. and Dubois F. (2013). Automated three-dimensional detection and classification of living organisms using digital holographic microscopy with partial spatial coherent source: application to the monitoring of drinking water resources. **Appl. Opt.** 52(1): A68-A80.

Merola, F., Miccio, L., Memmolo, P., Di Caprio, G. and Galli, A. (2013). Digital holography as a method for 3D imaging and estimating the biovolume of motile cells. **Lab on a Chip.** 23: 4512-4516.

Moon, I., Javidi, B., Yi, F., Boss, D. and Marquet, P. (2012). Automated statistical quantification of three-dimensional morphology and mean corpuscular hemoglobin of multiple red blood cells. **Opt. Exp.** 20(9): 10295-10309.

Moon, I., Yi, F. and Javidi, B. (2010). Automated three-dimensional microbial sensing and recognition using digital holography and statistical sampling. **Sensors.** 10: 8437-8451.

Morrison, K. E. (1995). Cosine products, Fourier transforms and random sums. **Am. Math Mon.** 102: 716-724.

Schnars, U. and Jüptner, W. (1994). Direct recording of holograms by a CCD target and numerical reconstruction. **Appl. Opt.** 33(2): 179-181.

Schnars, U. and Jüptner, W. (2005). **Digital holography-digital hologram recording, numerical reconstruction and related techniques.** Springer: New York.

Soontaranon, S., Widjaja, J. and Asakura, T. (2002). Direct analysis of in-line particle holograms by using wavelet transform and envelope reconstruction method. **Optik.** 113: 489-494.

Soontaranon, S., Widjaja, J. and Asakura, T. (2008). Extraction of object position from in-line holograms by using single wavelet coefficient. **Opt. Commun.** 281: 1461-1467.

Thompson, B. J. (1974). Holographic particle sizing technique. **J. Physics E. Sci. Inst.** 7: 781-788.

Tyler, G. A. and Thompson, B. J. (1976). Fraunhofer holography applied to particle size analysis: a reassessment. **Opt. Acta.** 23: 685-700.

Widjaja, J. and Chuamchaitrakool, P. (2013). Holographic particle tracking using Wigner-Ville distribution. **Opt. Lasers Eng.** 51: 311-316.

Widjaja, J. and Soontaranon, S. (2009). All wavelet analysis of in-line particle holograms. **Opt. Lasers Eng.** 47: 1325-1333.

Widjaja, J., Uozumi, J., Ushizaka, T. and Asakura, T. (1992). Real-time generation of the Wigner distribution function by means of a single acousto-optic modulator. **Opt. Commun.** 94: 313-320.

Yu, X., Hong, J., Liu, C., Cross, M., Haynie, D. T. and Kim, M. K. (2014). Four-dimensional motility tracking of biological cells by digital holographic microscopy. **Biomed. Opt. J.** 19: 045001.
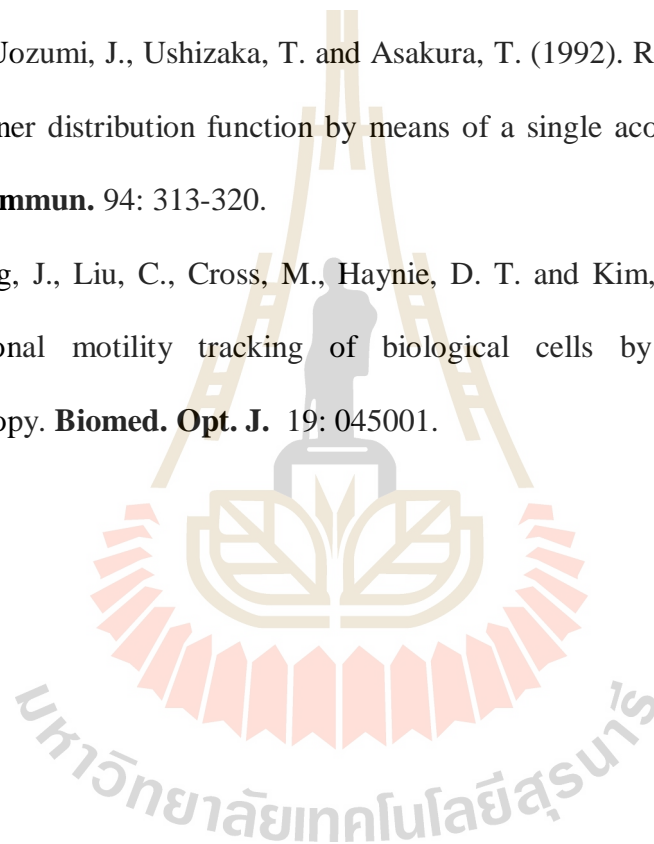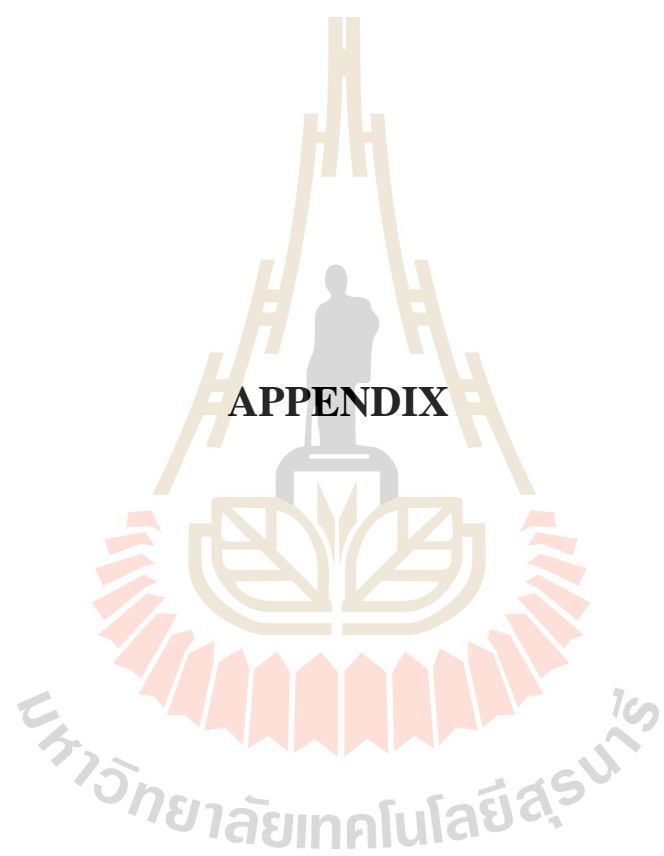
APPENDIX

APPENDIX

DERIVATION OF Eq. (3.4) – Eq. (3.7)

Recall the simplified in-line hologram given by Eq. (3.1) is

$$I(x) = \cos\left(\frac{\pi x^2}{\lambda z} - \frac{\pi}{4}\right) \left(\frac{\sin\left(\frac{2\pi a x}{\lambda z}\right)}{\frac{2\pi a x}{\lambda z}}\right) \text{rect}\left(\frac{x - \frac{L}{2}}{L}\right). \tag{A1}$$

Approximation of the sinc function by a product of three cosine terms gives

$$\text{sinc}(2f_0 x) = \prod_{n=1}^{3} \cos\left(\frac{2\pi f_0 x}{2^n}\right) = \cos\left(\frac{2\pi f_0 x}{2^1}\right)\cos\left(\frac{2\pi f_0 x}{2^2}\right)\cos\left(\frac{2\pi f_0 x}{2^3}\right), \tag{A2}$$

where $f_0 = a/\lambda z$. The sinc and the cosine chirp functions can be re-written by using the Euler's identity as

$$\text{sinc}(2f_0 x) = \frac{1}{8}\left\{\exp\left[j2\pi\left(\frac{7}{8}f_0\right)x\right] + \exp\left[-j2\pi\left(\frac{7}{8}f_0\right)x\right]\right.$$

$$+ \exp\left[j2\pi\left(\frac{5}{8}f_0\right)x\right] + \exp\left[-j2\pi\left(\frac{5}{8}f_0\right)x\right]$$

$$+ \exp\left[j2\pi\left(\frac{3}{8}f_0\right)x\right] + \exp\left[-j2\pi\left(\frac{3}{8}f_0\right)x\right]$$

$$\left. + \exp\left[j2\pi\left(\frac{1}{8}f_0\right)x\right] + \exp\left[-j2\pi\left(\frac{1}{8}f_0\right)x\right]\right\} \tag{A3}$$

and

$$\cos\left(\frac{\pi x^2}{\lambda z} - \frac{\pi}{4}\right) = \frac{1}{2}\left\{\exp\left[j\left(\beta\pi x^2 - \frac{\pi}{4}\right)\right] + \exp\left[-j\left(\beta\pi x^2 - \frac{\pi}{4}\right)\right]\right\}, \tag{A4}$$

respectively, with $\beta = 1/\lambda z$. Substitutions of Eqs. (A3) and (A4) into Eq. (A1) result in the simplified hologram as

$$I(x) = \frac{1}{16}\left\{\exp\left[j\left(\beta\pi x^2 - \frac{\pi}{4}\right)\right] + \exp\left[-j\left(\beta\pi x^2 - \frac{\pi}{4}\right)\right]\right\}$$

$$\times\left\{\exp\left[j2\pi\left(\frac{7}{8}f_0\right)x\right] + \exp\left[-j2\pi\left(\frac{7}{8}f_0\right)x\right]\right.$$

$$+ \exp\left[j2\pi\left(\frac{5}{8}f_0\right)x\right] + \exp\left[-j2\pi\left(\frac{5}{8}f_0\right)x\right]$$

$$+ \exp\left[j2\pi\left(\frac{3}{8}f_0\right)x\right] + \exp\left[-j2\pi\left(\frac{3}{8}f_0\right)x\right]$$

$$\left. + \exp\left[j2\pi\left(\frac{1}{8}f_0\right)x\right] + \exp\left[-j2\pi\left(\frac{1}{8}f_0\right)x\right]\right\}\mathrm{rect}\left(\frac{x-L/2}{L}\right). \qquad (A5)$$

Equation (A5) can be further expressed as

$$I(x) = \frac{1}{16}\left\{\exp\left[j2\pi f_0\left(\frac{7}{8}x + \frac{\beta x^2}{2f_0} - \frac{1}{8f_0}\right)\right] + \exp\left[j2\pi f_0\left(\frac{5}{8}x + \frac{\beta x^2}{2f_0} - \frac{1}{8f_0}\right)\right]\right.$$

$$+ \exp\left[j2\pi f_0\left(\frac{3}{8}x + \frac{\beta x^2}{2f_0} - \frac{1}{8f_0}\right)\right] + \exp\left[j2\pi f_0\left(\frac{1}{8}x + \frac{\beta x^2}{2f_0} - \frac{1}{8f_0}\right)\right]$$

$$+ \exp\left[j2\pi f_0\left(\frac{7}{8}x - \frac{\beta x^2}{2f_0} + \frac{1}{8f_0}\right)\right] + \exp\left[j2\pi f_0\left(\frac{5}{8}x - \frac{\beta x^2}{2f_0} + \frac{1}{8f_0}\right)\right]$$

$$+ \exp\left[j2\pi f_0\left(\frac{3}{8}x - \frac{\beta x^2}{2f_0} + \frac{1}{8f_0}\right)\right] + \exp\left[j2\pi f_0\left(\frac{1}{8}x - \frac{\beta x^2}{2f_0} + \frac{1}{8f_0}\right)\right]$$

$$+ \exp\left[j2\pi f_0\left(-\frac{7}{8}x + \frac{\beta x^2}{2f_0} - \frac{1}{8f_0}\right)\right] + \exp\left[j2\pi f_0\left(-\frac{5}{8}x + \frac{\beta x^2}{2f_0} - \frac{1}{8f_0}\right)\right]$$

$$+ \exp\left[j2\pi f_0\left(-\frac{3}{8}x + \frac{\beta x^2}{2f_0} - \frac{1}{8f_0}\right)\right] + \exp\left[j2\pi f_0\left(-\frac{1}{8}x + \frac{\beta x^2}{2f_0} - \frac{1}{8f_0}\right)\right]$$

$$+ \exp\left[j2\pi f_0 \left(-\frac{7}{8}x - \frac{\beta x^2}{2f_0} + \frac{1}{8f_0} \right)\right] + \exp\left[j2\pi f_0 \left(-\frac{5}{8}x - \frac{\beta x^2}{2f_0} + \frac{1}{8f_0} \right)\right]$$

$$+ \exp\left[j2\pi f_0 \left(-\frac{3}{8}x - \frac{\beta x^2}{2f_0} + \frac{1}{8f_0} \right)\right] + \exp\left[j2\pi f_0 \left(-\frac{1}{8}x - \frac{\beta x^2}{2f_0} + \frac{1}{8f_0} \right)\right]\Bigg\}$$

$$\times \mathrm{rect}\left(\frac{x - L/2}{L} \right). \tag{A6}$$

In order to obtain the analytic expression of Eq. (A6), the values of β, f_0 and x are substituted into each exponential component. The maximum value of x is $L = 4.15$ mm, which corresponds to the hologram size being analyzed. As x increases, the exponential components that give the positive value are determined for the analytic function. For simplicity of the derivation, the amplitude factor of $I(x)$ is neglected. Thus, the analytic function of the simplified in-line hologram becomes

$$I_a(x) = \Bigg\{ \exp\left[j2\pi f_0 \left(\frac{7}{8}x + \frac{\beta x^2}{2f_0} - \frac{1}{8f_0} \right)\right] + \exp\left[j2\pi f_0 \left(-\frac{7}{8}x + \frac{\beta x^2}{2f_0} - \frac{1}{8f_0} \right)\right]$$

$$+ \exp\left[j2\pi f_0 \left(\frac{5}{8}x + \frac{\beta x^2}{2f_0} - \frac{1}{8f_0} \right)\right] + \exp\left[j2\pi f_0 \left(-\frac{5}{8}x + \frac{\beta x^2}{2f_0} - \frac{1}{8f_0} \right)\right]$$

$$+ \exp\left[j2\pi f_0 \left(\frac{3}{8}x + \frac{\beta x^2}{2f_0} - \frac{1}{8f_0} \right)\right] + \exp\left[j2\pi f_0 \left(-\frac{3}{8}x + \frac{\beta x^2}{2f_0} - \frac{1}{8f_0} \right)\right]$$

$$+ \exp\left[j2\pi f_0 \left(\frac{1}{8}x + \frac{\beta x^2}{2f_0} - \frac{1}{8f_0} \right)\right] + \exp\left[j2\pi f_0 \left(-\frac{1}{8}x + \frac{\beta x^2}{2f_0} - \frac{1}{8f_0} \right)\right]\Bigg\}$$

$$\times \mathrm{rect}\left(\frac{x - L/2}{L} \right). \tag{A7}$$

The WVD output of the in-line hologram is derived by substituting the analytic function of Eq. (A7) into Eq. (2.5)

$$W_{Ia}(x, f_x) = \int_{-\infty}^{+\infty} I_a(x + \xi/2) I_a^*(x - \xi/2) \exp(-j2\pi f_x \xi) d\xi , \tag{A8}$$

where $I_a(x + \xi/2)$ is given by

$$
\begin{aligned}
I_a(x + \xi/2) = \Bigg\{ &\exp\left\{ j2\pi f_0 \left[\frac{7}{8}\left(x + \frac{\xi}{2}\right) + \frac{\beta}{2f_0}\left(x + \frac{\xi}{2}\right)^2 - \frac{1}{8f_0} \right] \right\} \\
&+ \exp\left\{ j2\pi f_0 \left[\frac{5}{8}\left(x + \frac{\xi}{2}\right) + \frac{\beta}{2f_0}\left(x + \frac{\xi}{2}\right)^2 - \frac{1}{8f_0} \right] \right\} \\
&+ \exp\left\{ j2\pi f_0 \left[\frac{3}{8}\left(x + \frac{\xi}{2}\right) + \frac{\beta}{2f_0}\left(x + \frac{\xi}{2}\right)^2 - \frac{1}{8f_0} \right] \right\} \\
&+ \exp\left\{ j2\pi f_0 \left[\frac{1}{8}\left(x + \frac{\xi}{2}\right) + \frac{\beta}{2f_0}\left(x + \frac{\xi}{2}\right)^2 - \frac{1}{8f_0} \right] \right\} \\
&+ \exp\left\{ j2\pi f_0 \left[-\frac{7}{8}\left(x + \frac{\xi}{2}\right) + \frac{\beta}{2f_0}\left(x + \frac{\xi}{2}\right)^2 - \frac{1}{8f_0} \right] \right\} \\
&+ \exp\left\{ j2\pi f_0 \left[-\frac{5}{8}\left(x + \frac{\xi}{2}\right) + \frac{\beta}{2f_0}\left(x + \frac{\xi}{2}\right)^2 - \frac{1}{8f_0} \right] \right\} \\
&+ \exp\left\{ j2\pi f_0 \left[-\frac{3}{8}\left(x + \frac{\xi}{2}\right) + \frac{\beta}{2f_0}\left(x + \frac{\xi}{2}\right)^2 - \frac{1}{8f_0} \right] \right\} \\
&+ \exp\left\{ j2\pi f_0 \left[-\frac{1}{8}\left(x + \frac{\xi}{2}\right) + \frac{\beta}{2f_0}\left(x + \frac{\xi}{2}\right)^2 - \frac{1}{8f_0} \right] \right\} \Bigg\} \\
&\times \mathrm{rect}\left(\frac{x - L/2}{L} \right) , \tag{A9}
\end{aligned}
$$

while $I_a^*(x - \xi/2)$ can be expressed as

$$I_a^*(x - \xi/2) = \left\{ \exp\left\{ -j2\pi f_0 \left[\frac{7}{8}\left(x - \frac{\xi}{2} \right) + \frac{\beta}{2f_0}\left(x - \frac{\xi}{2} \right)^2 - \frac{1}{8f_0} \right] \right\} \right.$$

$$+ \exp\left\{ -j2\pi f_0 \left[\frac{5}{8}\left(x - \frac{\xi}{2} \right) + \frac{\beta}{2f_0}\left(x - \frac{\xi}{2} \right)^2 - \frac{1}{8f_0} \right] \right\}$$

$$+ \exp\left\{ -j2\pi f_0 \left[\frac{3}{8}\left(x - \frac{\xi}{2} \right) + \frac{\beta}{2f_0}\left(x - \frac{\xi}{2} \right)^2 - \frac{1}{8f_0} \right] \right\}$$

$$+ \exp\left\{ -j2\pi f_0 \left[\frac{1}{8}\left(x - \frac{\xi}{2} \right) + \frac{\beta}{2f_0}\left(x - \frac{\xi}{2} \right)^2 - \frac{1}{8f_0} \right] \right\}$$

$$+ \exp\left\{ -j2\pi f_0 \left[-\frac{7}{8}\left(x - \frac{\xi}{2} \right) + \frac{\beta}{2f_0}\left(x - \frac{\xi}{2} \right)^2 - \frac{1}{8f_0} \right] \right\}$$

$$+ \exp\left\{ -j2\pi f_0 \left[-\frac{5}{8}\left(x - \frac{\xi}{2} \right) + \frac{\beta}{2f_0}\left(x - \frac{\xi}{2} \right)^2 - \frac{1}{8f_0} \right] \right\}$$

$$+ \exp\left\{ -j2\pi f_0 \left[-\frac{3}{8}\left(x - \frac{\xi}{2} \right) + \frac{\beta}{2f_0}\left(x - \frac{\xi}{2} \right)^2 - \frac{1}{8f_0} \right] \right\}$$

$$\left. + \exp\left\{ -j2\pi f_0 \left[-\frac{1}{8}\left(x - \frac{\xi}{2} \right) + \frac{\beta}{2f_0}\left(x - \frac{\xi}{2} \right)^2 - \frac{1}{8f_0} \right] \right\} \right\}$$

$$\times \mathrm{rect}\left(\frac{x - L/2}{L} \right). \tag{A10}$$

For the sake of simplicity, Eqs. (A9) and (A10) are re-expressed as

$$I_a(x + \xi/2) = \sum_{m=1}^{8} \exp\left\{ j2\pi f_0 \left[A_m\left(x + \frac{\xi}{2} \right) + \frac{\beta}{2f_0}\left(x + \frac{\xi}{2} \right)^2 - \frac{1}{8f_0} \right] \right\}$$

$$\times \mathrm{rect}\left(\frac{x - L/2}{L} \right) \tag{A11}$$

and

$$I_a^*(x - \xi/2) = \sum_{n=1}^{8} \exp\left\{- j2\pi f_0\left[B_m\left(x - \frac{\xi}{2}\right) + \frac{\beta}{2f_0}\left(x - \frac{\xi}{2}\right)^2 - \frac{1}{8f_0}\right]\right\}$$

$$\times \mathrm{rect}\left(\frac{x - L/2}{L}\right), \tag{A12}$$

respectively. The factor A_m and B_m are defined as $\left\{2^M - [1 + 2(m-1)]\right\}/2^M$, where M is equal to 3 and m is the natural number $1,2,3,\ldots,\ 2^M$. Consequently, the autocorrelation $I_a(x + \xi/2)I_a^*(x - \xi/2)$ can be expressed as

$$I_a(x + \xi/2)I_a^*(x - \xi/2) = \exp\left\{ j2\pi f_0\left[(A_m - B_m)x + (A_m + B_m)\frac{\xi}{2} + \frac{\beta x \xi}{f_0}\right]\right\}$$

$$\times \mathrm{rect}\left(\frac{x - L/2}{L}\right), \tag{A13}$$

which consists of sixty-four exponential terms.

The WVD of Eq. (A1) is calculated by taking Fourier transform of Eq. (A13) with the boundary of the integration from $-(L - 2|x - L/2|)$ to $(L - 2|x - L/2|)$. Thus, the WVD of the simplified hologram is

$$W_{Ia}(x, f_x) = \int_{-(L - 2|x - L/2|)}^{L - 2|x - L/2|} \exp\left\{ j2\pi f_0\left[(A_m - B_m)x + (A_m + B_m)\frac{\xi}{2} + \frac{\beta x \xi}{f_0}\right]\right\}$$

$$\times \exp(- j2\pi f_x \xi)d\xi. \tag{A14}$$

The solution of Eq. (A14) is shown as follows.

$$W_{Ia}(x, f_x) = \exp[j2\pi f_0(A_m - B_m)x]$$

$$\times \int_{-L - 2|x - L/2|}^{L - 2|x - L/2|} \exp\left\{ - j2\pi \xi\left[f_x - (A_m + B_m)\frac{f_0}{2} - \beta x\right]\right\}d\xi \tag{A15}$$

$$= - \exp[j2\pi f_0(A_m - B_m)x]\bigg/ j2\pi\left[f_x - (A_m + B_m)\frac{f_0}{2} - \beta x\right]$$

$$\times \exp\left\{ -j2\pi\left(L - 2\left|x - \frac{L}{2}\right|\right) \times \left[f_x - (A_m + B_m)\frac{f_0}{2} - \beta x\right]\right.$$

$$\left. -\exp j2\pi\left(L - 2\left|x - \frac{L}{2}\right|\right) \times \left[f_x - (A_m + B_m)\frac{f_0}{2} - \beta x\right]\right\}$$

$$= \left\{\exp\left\{-j2\pi\left(L - 2\left|x - \frac{L}{2}\right|\right) \times \left[f_x - (A_m + B_m)\frac{f_0}{2} - \beta x\right]\right\}\middle/ 2j\right.$$

$$\left. -\exp\left\{j2\pi\left(L - 2\left|x - \frac{L}{2}\right|\right) \times \left[f_x - (A_m + B_m)\frac{f_0}{2} - \beta x\right]\right\}\middle/ 2j\right\}$$

$$\times \left(\frac{\exp[j2\pi f_0 (A_m - B_m)x]}{\pi\left\{f_x - (A_m + B_m)\frac{f_0}{2} - \beta x\right\}}\right)$$

$$= \left\{\frac{\exp[j2\pi f_0 (A_m - B_m)x]}{\pi\left[f_x - (A_m + B_m)\frac{f_0}{2} - \beta x\right]}\sin\left\{2\pi\left(L - 2\left|x - \frac{L}{2}\right|\right) \times \left[f_x - (A_m + B_m)\frac{f_0}{2} - \beta x\right]\right\}\right\}$$

$$= \left[2\left(L - 2\left|x - \frac{L}{2}\right|\right)\right]\exp[j2\pi f_0 (A_m - B_m)x]\left\{\frac{\sin\left\{2\pi\left(L - 2\left|x - \frac{L}{2}\right|\right) \times \left[f_x - (A_m + B_m)\frac{f_0}{2} - \beta x\right]\right\}}{2\pi\left(L - 2\left|x - \frac{L}{2}\right|\right) \times \left[f_x - (A_m + B_m)\frac{f_0}{2} - \beta x\right]}\right\}$$

$$W_{Ia}(x, f_x) = \exp[j2\pi f_0 (A_m - B_m)x] \times \left[2\left(L - 2\left|x - \frac{L}{2}\right|\right)\right]$$

$$\times \operatorname{sinc}\left\{2\left(L - 2\left|x - \frac{L}{2}\right|\right) \times \left[f_x - (A_m + B_m)\frac{f_0}{2} - \beta x\right]\right\}. \tag{A16}$$

Table A1 shows the values of A_m+B_m and A_m-B_m.

WVD component W_{Ia}	Values of A_m+B_m	Values of A_m-B_m							
1	14/8	0							
2	12/8		±2/8						
3	10/8	0		±4/8					
4	8/8		±2/8		±6/8				
5	6/8	0		±4/8		±8/8			
6	4/8		±2/8		±6/8		±10/8		
7	2/8	0		±4/8		±8/8		±12/8	
8	0/8		±2/8		±6/8		±10/8		±14/8
9	-2/8	0		±4/8		±8/8		±12/8	
10	-4/8		±2/8		±6/8		±10/8		
11	-6/8	0		±4/8		±8/8			
12	-8/8		±2/8		±6/8				
13	-10/8	0		±4/8					
14	-12/8		±2/8						
15	-14/8	0							

A substitution of A_m–B_m into the exponential term of Eq. (A16) results in a conjugate pair of exponential functions. This indicates that Eq. (A16) can be further simplified into a cosine function. The WVD output of a simplified in-line hologram can be expressed as

$$W_{Ia}(x, f_x) = 2\cos[2\pi f_0 x(A_m - B_m)] \times \left[2\left(L - 2\left|x - \frac{L}{2}\right|\right)\right]$$

$$\times \text{sinc}\left\{\left[2\left(L - 2\left|x - \frac{L}{2}\right|\right)\right] \times \left[f_x - (A_m + B_m)\frac{f_0}{2} - \beta x\right]\right\}. \quad (A17)$$

By substituting the values of A_m+B_m and A_m–B_m in Table A1 into Eq. (A17), the fifteen WVD components become

$$W_{Ia1}(x, f_x) = 2(L - 2|x - L/2|)\text{sinc}\{2(L - 2|x - L/2|) \times [f_x - f_0(7/8) - \beta x]\} \quad (A18.1)$$

$$W_{Ia2}(x, f_x) = \{2\cos[2\pi f_0 x(2/8)]\} \times [2(L - 2|x - L/2|)]$$

$$\times \text{sinc}\{2(L - 2|x - L/2|) \times [f_x - f_0(6/8) - \beta x]\} \quad (A18.2)$$

$$W_{Ia3}(x, f_x) = \{1 + 2\cos[2\pi f_0 x(4/8)]\} \times [2(L - 2|x - L/2|)]$$

$$\times \text{sinc}\{2(L - 2|x - L/2|) \times [f_x - f_0(5/8) - \beta x]\} \quad (A18.3)$$

$$W_{Ia4}(x, f_x) = \{2\cos[2\pi f_0 x(6/8)] + 2\cos[2\pi f_0 x(2/8)]\} \times [2(L - 2|x - L/2|)]$$

$$\times \text{sinc}\{2(L - 2|x - L/2|) \times [f_x - f_0(4/8) - \beta x]\} \quad (A18.4)$$

$$W_{Ia5}(x, f_x) = \{1 + 2\cos[2\pi f_0 x(8/8)] + 2\cos[2\pi f_0 x(4/8)]\}$$

$$\times [2(L - 2|x - L/2|)] \times \mathrm{sinc}\{2(L - 2|x - L/2|) \times [f_x - f_0(3/8) - \beta x]\} \quad \text{(A18.5)}$$

$$W_{Ia6}(x, f_x) = \{2\cos[2\pi f_0 x(10/8)] + 2\cos[2\pi f_0 x(6/8)] + 2\cos[2\pi f_0 x(2/8)]\}$$

$$\times [2(L - 2|x - L/2|)] \times \mathrm{sinc}\{2(L - 2|x - L/2|) \times [f_x - f_0(2/8) - \beta x]\} \quad \text{(A18.6)}$$

$$W_{Ia7}(x, f_x) = \{1 + 2\cos[2\pi f_0 x(12/8)] + 2\cos[2\pi f_0 x(8/8)] + 2\cos[2\pi f_0 x(4/8)]\}$$

$$\times [2(L - 2|x - L/2|)] \times \mathrm{sinc}\{2(L - 2|x - L/2|) \times [f_x - f_0(1/8) - \beta x]\} \quad \text{(A18.7)}$$

$$W_{Ia8}(x, f_x) = \{2\cos[2\pi f_0 x(14/8)] + 2\cos[2\pi f_0 x(10/8)] + 2\cos[2\pi f_0 x(6/8)]$$

$$+ 2\cos[2\pi f_0 x(2/8)]\} \times [2(L - 2|x - L/2|)]$$

$$\times \mathrm{sinc}[2(L - 2|x - L/2|) \times (f_x - \beta x)] \quad \text{(A18.8)}$$

$$W_{Ia9}(x, f_x) = \{1 + 2\cos[2\pi f_0 x(12/8)] + 2\cos[2\pi f_0 x(8/8)] + 2\cos[2\pi f_0 x(4/8)]\}$$

$$\times [2(L - 2|x - L/2|)] \times \mathrm{sinc}\{2(L - 2|x - L/2|) \times [f_x + f_0(1/8) - \beta x]\} \quad \text{(A18.9)}$$

$$W_{Ia10}(x, f_x) = \{2\cos[2\pi f_0 x(10/8)] + 2\cos[2\pi f_0 x(6/8)] + 2\cos[2\pi f_0 x(2/8)]\}$$

$$\times [2(L - 2|x - L/2|)] \times \mathrm{sinc}\{2(L - 2|x - L/2|) \times [f_x + f_0(2/8) - \beta x]\} \quad \text{(A18.10)}$$

$$W_{Ia11}(x, f_x) = \{1 + 2\cos[2\pi f_0 x(8/8)] + 2\cos[2\pi f_0 x(4/8)]\}$$

$$\times 2(L - 2|x - L/2|) \times \mathrm{sinc}\{2(L - 2|x - L/2|) \times [f_x + f_0(3/8) - \beta x]\} \quad \text{(A18.11)}$$

$$W_{Ia12}(x, f_x) = \{2\cos[2\pi f_0 x(6/8)] + 2\cos[2\pi f_0 x(2/8)]\}$$

$$\times [2(L - 2|x - L/2|)] \times \text{sinc}\{2(L - 2|x - L/2|) \times [f_x + f_0(4/8) - \beta x]\} \quad \text{(A18.12)}$$

$$W_{Ia13}(x, f_x) = \{1 + 2\cos[2\pi f_0 x(4/8)]\} \times [2(L - 2|x - L/2|)]$$

$$\times \text{sinc}\{2(L - 2|x - L/2|) \times [f_x + f_0(5/8) - \beta x]\} \quad \text{(A18.13)}$$

$$W_{Ia14}(x, f_x) = [2\cos(2\pi f_0 x(2/8))] \times [2(L - 2|x - L/2|)]$$

$$\times \text{sinc}\{2(L - 2|x - L/2|) \times [f_x + f_0(6/8) - \beta x]\} \quad \text{(A18.14)}$$

$$W_{Ia15}(x, f_x) = [2(L - 2|x - L/2|)] \times \text{sinc}\{2(L - 2|x - L/2|) \times [f_x + f_0(7/8) - \beta x]\}. \quad \text{(A18.15)}$$

In the case of the sinc approximation by using N cosine terms, the general expression of the WVD components is given by

$$W_{I_a}(x, f_x) = \sum_{k=1}^{2^{N+1}-1}\left[\sum_{m=1}^{k}(-1)^m + \sum_n 2\cos\left\{2\pi x f_0\left[\frac{2^{N+1} - 2(|2^N - n| + 1)}{2^N}\right]\right\}\right]$$

$$\times 2(L - 2|x - L/2|) \times \text{sinc}\left\{2(L - 2|x - L/2|)\left[f_x - \left(\frac{2^N - k}{2^N}\right)f_0 - \beta x\right]\right\}, \quad \text{(A19)}$$

For the case of $N = 5$, there are sixty-three WVD components that are

$$W_{Ia1}(x, f_x) = [2(L - 2|x - L/2|)] \times \text{sinc}\{2(L - 2|x - L/2|) \times [f_x - f_0(62/64) - \beta x]\} \quad \text{(A19.1)}$$

$$W_{Ia2}(x, f_x) = \{2\cos[2\pi f_0 x(2/32)]\} \times [2(L - 2|x - L/2|)]$$

$$\times \operatorname{sinc}\{2(L - 2|x - L/2|) \times [f_x - f_0(60/64) - \beta x]\} \quad \text{(A19.2)}$$

$$W_{Ia3}(x, f_x) = \{1 + 2\cos[2\pi f_0 x(4/32)]\} \times [2(L - 2|x - L/2|)]$$

$$\times \operatorname{sinc}\{2(L - 2|x - L/2|) \times [f_x - f_0(58/64) - \beta x]\} \quad \text{(A19.3)}$$

$$W_{Ia4}(x, f_x) = \{2\cos[2\pi f_0 x(2/32)] + 2\cos[2\pi f_0 x(6/32)]\} \times [2(L - 2|x - L/2|)]$$

$$\times \operatorname{sinc}\{2(L - 2|x - L/2|) \times [f_x - f_0(56/64) - \beta x]\} \quad \text{(A19.4)}$$

$$W_{Ia5}(x, f_x) = \{1 + 2\cos(2\pi f_0 x(4/32)) + 2\cos(2\pi f_0 x(8/32))\} \times [2(L - 2|x - L/2|)]$$

$$\times \operatorname{sinc}\{2(L - 2|x - L/2|) \times [f_x - f_0(54/64) - \beta x]\} \quad \text{(A19.5)}$$

$$W_{Ia6}(x, f_x) = \{2\cos[2\pi f_0 x(2/32)] + 2\cos[2\pi f_0 x(6/32)] + 2\cos[2\pi f_0 x(10/32)]\}$$

$$\times [2(L - 2|x - L/2|)] \times \operatorname{sinc}\{2(L - 2|x - L/2|)[f_x - f_0(52/64) - \beta x]\} \quad \text{(A19.6)}$$

$$W_{Ia7}(x, f_x) = \{1 + 2\cos[2\pi f_0 x(4/32)] + 2\cos[2\pi f_0 x(8/32)] + 2\cos[2\pi f_0 x(12/32)]\}$$

$$\times [2(L - 2|x - L/2|)] \times \operatorname{sinc}\{2(L - 2|x - L/2|) \times [f_x - f_0(50/64) - \beta x]\} \quad \text{(A19.7)}$$

$$W_{Ia8}(x, f_x) = \{2\cos[2\pi f_0 x(2/32)] + 2\cos[2\pi f_0 x(6/32)] + 2\cos[2\pi f_0 x(10/32)]$$

$$+ 2\cos[2\pi f_0 x(14/32)]\} \times [2(L - 2|x - L/2|)]$$

$$\times \operatorname{sinc}\{2(L - 2|x - L/2|) \times [f_x - f_0(48/64) - \beta x]\} \quad \text{(A19.8)}$$

$$W_{Ia9}(x, f_x) = \{1 + 2\cos[2\pi f_0 x(4/32)] + 2\cos[2\pi f_0 x(8/32)] + 2\cos[2\pi f_0 x(12/32)]$$

$$+ 2\cos[2\pi f_0 x(16/32)]\} \times [2(L - 2|x - L/2|)]$$

$$\times \text{sinc}\{2(L - 2|x - L/2|) \times [f_x - f_0(46/64) - \beta x]\} \tag{A19.9}$$

$$W_{Ia10}(x, f_x) = \{2\cos[2\pi f_0 x(2/32)] + 2\cos[2\pi f_0 x(6/32)] + 2\cos[2\pi f_0 x(10/32)]$$

$$+ 2\cos[2\pi f_0 x(14/32)] + 2\cos[2\pi f_0 x(18/32)]\} \times [2(L - 2|x - L/2|)]$$

$$\times \text{sinc}\{2(L - 2|x - L/2|) \times [f_x - f_0(44/64) - \beta x]\} \tag{A19.10}$$

$$W_{Ia11}(x, f_x) = \{1 + 2\cos[2\pi f_0 x(4/32)] + 2\cos[2\pi f_0 x(8/32)] + 2\cos[2\pi f_0 x(12/32)]$$

$$+ 2\cos[2\pi f_0 x(16/32)] + 2\cos[2\pi f_0 x(20/32)]\} \times [2(L - 2|x - L/2|)]$$

$$\times \text{sinc}\{2(L - 2|x - L/2|) \times [f_x - f_0(42/64) - \beta x]\} \tag{A19.11}$$

$$W_{Ia12}(x, f_x) = \{2\cos[2\pi f_0 x(2/32)] + 2\cos[2\pi f_0 x(6/32)] + 2\cos[2\pi f_0 x(10/32)]$$

$$+ 2\cos[2\pi f_0 x(14/32)] + 2\cos[2\pi f_0 x(18/32)] + 2\cos[2\pi f_0 x(22/32)]\}$$

$$\times [2(L - 2|x - L/2|)] \times \text{sinc}\{2(L - 2|x - L/2|) \times [f_x - f_0(40/64) - \beta x]\} \tag{A19.12}$$

$$W_{Ia13}(x, f_x) = \{1 + 2\cos[2\pi f_0 x(4/32)] + 2\cos[2\pi f_0 x(8/32)] + 2\cos[2\pi f_0 x(12/32)]$$

$$+ 2\cos[2\pi f_0 x(16/32)] + 2\cos[2\pi f_0 x(20/32)] + 2\cos[2\pi f_0 x(24/32)]\}$$

$$\times [2(L - 2|x - L/2|)] \times \text{sinc}\{2(L - 2|x - L/2|) \times [f_x - f_0(38/64) - \beta x]\} \tag{A19.13}$$

$$W_{Ia14}(x, f_x) = \{2\cos[2\pi f_0 x(2/32)] + 2\cos[2\pi f_0 x(6/32)] + 2\cos[2\pi f_0 x(10/32)]$$

$$+ 2\cos[2\pi f_0 x(14/32)] + 2\cos[2\pi f_0 x(18/32)] + 2\cos[2\pi f_0 x(22/32)]$$

$$+ 2\cos[2\pi f_0 x(26/32)]\} \times [2(L - 2|x - L/2|)]$$

$$\times \text{sinc}\{2(L - 2|x - L/2|) \times [f_x - f_0(36/64) - \beta x]\} \qquad (A19.14)$$

$$W_{Ia15}(x, f_x) = \{1 + 2\cos[2\pi f_0 x(4/32)] + 2\cos[2\pi f_0 x(8/32)] + 2\cos[2\pi f_0 x(12/32)]$$

$$+ 2\cos[2\pi f_0 x(16/32)] + 2\cos[2\pi f_0 x(20/32)] + 2\cos[2\pi f_0 x(24/32)]$$

$$+ 2\cos[2\pi f_0 x(28/32)]\} \times [2(L - 2|x - L/2|)]$$

$$\times \text{sinc}\{2(L - 2|x - L/2|) \times [f_x - f_0(34/64) - \beta x]\} \qquad (A19.15)$$

$$W_{Ia16}(x, f_x) = \{2\cos[2\pi f_0 x(2/32)] + 2\cos[2\pi f_0 x(6/32)] + 2\cos[2\pi f_0 x(10/32)]$$

$$+ 2\cos[2\pi f_0 x(14/32)] + 2\cos[2\pi f_0 x(18/32)] + 2\cos[2\pi f_0 x(22/32)]$$

$$+ 2\cos[2\pi f_0 x(26/32)] + 2\cos[2\pi f_0 x(30/32)]\} \times [2(L - 2|x - L/2|)]$$

$$\times \text{sinc}\{2(L - 2|x - L/2|) \times [f_x - f_0(32/64) - \beta x]\} \qquad (A19.16)$$

$$W_{Ia17}(x, f_x) = \{1 + 2\cos[2\pi f_0 x(4/32)] + 2\cos[2\pi f_0 x(8/32)] + 2\cos[2\pi f_0 x(12/32)]$$

$$+ 2\cos[2\pi f_0 x(16/32)] + 2\cos[2\pi f_0 x(20/32)] + 2\cos[2\pi f_0 x(24/32)]$$

$$+ 2\cos[2\pi f_0 x(28/32)] + 2\cos[2\pi f_0 x(32/32)]\} \times [2(L - 2|x - L/2|)]$$

$$\times \text{sinc}\{2(L - 2|x - L/2|) \times [f_x - f_0(30/64) - \beta x]\} \qquad (A19.17)$$

$$W_{Ia18}(x, f_x) = \{2\cos[2\pi f_0 x(2/32)] + 2\cos[2\pi f_0 x(6/32)] + 2\cos[2\pi f_0 x(10/32)]$$

$$+ 2\cos[2\pi f_0 x(14/32)] + 2\cos[2\pi f_0 x(18/32)] + 2\cos[2\pi f_0 x(22/32)]$$

$$+ 2\cos[2\pi f_0 x(26/32)] + 2\cos[2\pi f_0 x(30/32)] + 2\cos[2\pi f_0 x(34/32)]\}$$

$$\times [2(L - 2|x - L/2|)] \times \text{sinc}\{2(L - 2|x - L/2|) \times [f_x - f_0(28/64) - \beta x]\} \quad \text{(A19.18)}$$

$$W_{Ia19}(x, f_x) = \{1 + 2\cos[2\pi f_0 x(4/32)] + 2\cos[2\pi f_0 x(8/32)] + 2\cos[2\pi f_0 x(12/32)]$$

$$+ 2\cos[2\pi f_0 x(16/32)] + 2\cos[2\pi f_0 x(20/32)] + 2\cos[2\pi f_0 x(24/32)]$$

$$+ 2\cos[2\pi f_0 x(28/32)] + 2\cos[2\pi f_0 x(32/32)] + 2\cos[2\pi f_0 x(36/32)]\}$$

$$\times [2(L - 2|x - L/2|)] \times \text{sinc}\{2(L - 2|x - L/2|) \times [f_x - f_0(26/64) - \beta x]\} \quad \text{(A19.19)}$$

$$W_{Ia20}(x, f_x) = \{2\cos[2\pi f_0 x(2/32)] + 2\cos[2\pi f_0 x(6/32)] + 2\cos[2\pi f_0 x(10/32)]$$

$$+ 2\cos[2\pi f_0 x(14/32)] + 2\cos[2\pi f_0 x(18/32)] + 2\cos[2\pi f_0 x(22/32)]$$

$$+ 2\cos[2\pi f_0 x(26/32)] + 2\cos[2\pi f_0 x(30/32)] + 2\cos[2\pi f_0 x(34/32)]$$

$$+ 2\cos[2\pi f_0 x(38/32)]\} \times [2(L - 2|x - L/2|)]$$

$$\times \text{sinc}\{2(L - 2|x - L/2|) \times [f_x - f_0(24/64) - \beta x]\} \quad \text{(A19.20)}$$

$$W_{Ia21}(x, f_x) = \{1 + 2\cos[2\pi f_0 x(4/32)] + 2\cos[2\pi f_0 x(8/32)] + 2\cos[2\pi f_0 x(12/32)]$$

$$+ 2\cos[2\pi f_0 x(16/32)] + 2\cos[2\pi f_0 x(20/32)] + 2\cos[2\pi f_0 x(24/32)]$$

$$+ 2\cos[2\pi f_0 x(28/32)] + 2\cos[2\pi f_0 x(32/32)] + 2\cos[2\pi f_0 x(36/32)]$$

$$+ 2\cos[2\pi f_0 x(40/32)]\} \times [2(L - 2|x - L/2|)]$$

$$\times \text{sinc}\{2(L - 2|x - L/2|) \times [f_x - f_0(22/64) - \beta x]\} \quad \text{(A19.21)}$$

$$W_{Ia22}(x, f_x) = \{2\cos[2\pi f_0 x(2/32)] + 2\cos[2\pi f_0 x(6/32)] + 2\cos[2\pi f_0 x(10/32)]$$

$$+ 2\cos[2\pi f_0 x(14/32)] + 2\cos[2\pi f_0 x(18/32)] + 2\cos[2\pi f_0 x(22/32)]$$

$$+ 2\cos[2\pi f_0 x(26/32)] + 2\cos[2\pi f_0 x(30/32)] + 2\cos[2\pi f_0 x(34/32)]$$

$$+ 2\cos[2\pi f_0 x(38/32)] + 2\cos[2\pi f_0 x(42/32)]\} \times [2(L - 2|x - L/2|)]$$

$$\times \mathrm{sinc}\{2(L - 2|x - L/2|) \times [f_x - f_0(20/64) - \beta x]\} \tag{A19.22}$$

$$W_{Ia23}(x, f_x) = \{1 + 2\cos[2\pi f_0 x(4/32)] + 2\cos[2\pi f_0 x(8/32)] + 2\cos[2\pi f_0 x(12/32)]$$

$$+ 2\cos[2\pi f_0 x(16/32)] + 2\cos[2\pi f_0 x(20/32)] + 2\cos[2\pi f_0 x(24/32)]$$

$$+ 2\cos[2\pi f_0 x(28/32)] + 2\cos[2\pi f_0 x(32/32)] + 2\cos[2\pi f_0 x(36/32)]$$

$$+ 2\cos[2\pi f_0 x(40/32)] + 2\cos[2\pi f_0 x(44/32)]\} \times [2(L - 2|x - L/2|)]$$

$$\times \mathrm{sinc}\{2(L - 2|x - L/2|) \times [f_x - f_0(18/64) - \beta x]\} \tag{A19.23}$$

$$W_{Ia24}(x, f_x) = \{2\cos[2\pi f_0 x(2/32)] + 2\cos[2\pi f_0 x(6/32)] + 2\cos[2\pi f_0 x(10/32)]$$

$$+ 2\cos[2\pi f_0 x(14/32)] + 2\cos[2\pi f_0 x(18/32)] + 2\cos[2\pi f_0 x(22/32)]$$

$$+ 2\cos[2\pi f_0 x(26/32)] + 2\cos[2\pi f_0 x(30/32)] + 2\cos[2\pi f_0 x(34/32)]$$

$$+ 2\cos[2\pi f_0 x(38/32)] + 2\cos[2\pi f_0 x(42/32)] + 2\cos[2\pi f_0 x(46/32)]\}$$

$$\times [2(L - 2|x - L/2|)] \times \mathrm{sinc}\{2(L - 2|x - L/2|) \times [f_x - f_0(16/64) - \beta x]\} \tag{A19.24}$$

$$W_{Ia25}(x, f_x) = \{1 + 2\cos[2\pi f_0 x(4/32)] + 2\cos[2\pi f_0 x(8/32)] + 2\cos[2\pi f_0 x(12/32)]$$

$$+ 2\cos[2\pi f_0 x(16/32)] + 2\cos[2\pi f_0 x(20/32)] + 2\cos[2\pi f_0 x(24/32)]$$

$$+ 2\cos\left[2\pi f_0 x(28/32)\right] + 2\cos\left[2\pi f_0 x(32/32)\right] + 2\cos\left[2\pi f_0 x(36/32)\right]$$

$$+ 2\cos\left[2\pi f_0 x(40/32)\right] + 2\cos\left[2\pi f_0 x(44/32)\right] + 2\cos\left[2\pi f_0 x(48/32)\right]\}$$

$$\times \left[2(L - 2|x - L/2|)\right] \times \mathrm{sinc}\left\{2(L - 2|x - L/2|) \times \left[f_x - f_0(14/64) - \beta x\right]\right\} \quad \text{(A19.25)}$$

$$W_{Ia26}(x, f_x) = \{2\cos\left[2\pi f_0 x(2/32)\right] + 2\cos\left[2\pi f_0 x(6/32)\right] + 2\cos\left[2\pi f_0 x(10/32)\right]$$

$$+ 2\cos\left[2\pi f_0 x(14/32)\right] + 2\cos\left[2\pi f_0 x(18/32)\right] + 2\cos\left[2\pi f_0 x(22/32)\right]$$

$$+ 2\cos\left[2\pi f_0 x(26/32)\right] + 2\cos\left[2\pi f_0 x(30/32)\right] + 2\cos\left[2\pi f_0 x(34/32)\right]$$

$$+ 2\cos\left[2\pi f_0 x(38/32)\right] + 2\cos\left[2\pi f_0 x(42/32)\right] + 2\cos\left[2\pi f_0 x(46/32)\right]$$

$$+ 2\cos\left[2\pi f_0 x(50/32)\right]\} \times \left[2(L - 2|x - L/2|)\right]$$

$$\times \mathrm{sinc}\left\{2(L - 2|x - L/2|) \times \left[f_x - f_0(12/64) - \beta x\right]\right\} \quad \text{(A19.26)}$$

$$W_{Ia27}(x, f_x) = \{1 + 2\cos\left[2\pi f_0 x(4/32)\right] + 2\cos\left[2\pi f_0 x(8/32)\right] + 2\cos\left[2\pi f_0 x(12/32)\right]$$

$$+ 2\cos\left[2\pi f_0 x(16/32)\right] + 2\cos\left[2\pi f_0 x(20/32)\right] + 2\cos\left[2\pi f_0 x(24/32)\right]$$

$$+ 2\cos\left[2\pi f_0 x(28/32)\right] + 2\cos\left[2\pi f_0 x(32/32)\right] + 2\cos\left[2\pi f_0 x(36/32)\right]$$

$$+ 2\cos\left[2\pi f_0 x(40/32)\right] + 2\cos\left[2\pi f_0 x(44/32)\right] + 2\cos\left[2\pi f_0 x(48/32)\right]$$

$$+ 2\cos(2\pi f_0 x(52/32))\} \times \left[2(L - 2|x - L/2|)\right]$$

$$\times \mathrm{sinc}\left\{2(L - 2|x - L/2|) \times \left[f_x - f_0(10/64) - \beta x\right]\right\} \quad \text{(A19.27)}$$

$$W_{Ia28}(x, f_x) = \{2\cos\left[2\pi f_0 x(2/32)\right] + 2\cos\left[2\pi f_0 x(6/32)\right] + 2\cos\left[2\pi f_0 x(10/32)\right]$$

$$+ 2\cos\left[2\pi f_0 x(14/32)\right] + 2\cos\left[2\pi f_0 x(18/32)\right] + 2\cos\left[2\pi f_0 x(22/32)\right]$$

$$+ 2\cos\left[2\pi f_0 x(26/32)\right] + 2\cos\left[2\pi f_0 x(30/32)\right] + 2\cos\left[2\pi f_0 x(34/32)\right]$$

$$+ 2\cos[2\pi f_0 x(38/32)] + 2\cos[2\pi f_0 x(42/32)] + 2\cos[2\pi f_0 x(46/32)]$$

$$+ 2\cos[2\pi f_0 x(50/32)] + 2\cos[2\pi f_0 x(54/32)]\} \times [2(L - 2|x - L/2|)]$$

$$\times \text{sinc}\{2(L - 2|x - L/2|) \times [f_x - f_0(8/64) - \beta x]\} \qquad (A19.28)$$

$$W_{Ia29}(x, f_x) = \{1 + 2\cos[2\pi f_0 x(4/32)] + 2\cos[2\pi f_0 x(8/32)] + 2\cos[2\pi f_0 x(12/32)]$$

$$+ 2\cos[2\pi f_0 x(16/32)] + 2\cos[2\pi f_0 x(20/32)] + 2\cos[2\pi f_0 x(24/32)]$$

$$+ 2\cos[2\pi f_0 x(28/32)] + 2\cos[2\pi f_0 x(32/32)] + 2\cos[2\pi f_0 x(36/32)]$$

$$+ 2\cos[2\pi f_0 x(40/32)] + 2\cos[2\pi f_0 x(44/32)] + 2\cos[2\pi f_0 x(48/32)]$$

$$+ 2\cos[2\pi f_0 x(52/32)] + 2\cos[2\pi f_0 x(56/32)]\} \times [2(L - 2|x - L/2|)]$$

$$\times \text{sinc}\{2(L - 2|x - L/2|) \times [f_x - f_0(6/64) - \beta x]\} \qquad (A19.29)$$

$$W_{Ia30}(x, f_x) = \{2\cos[2\pi f_0 x(2/32)] + 2\cos[2\pi f_0 x(6/32)] + 2\cos[2\pi f_0 x(10/32)]$$

$$+ 2\cos[2\pi f_0 x(14/32)] + 2\cos[2\pi f_0 x(18/32)] + 2\cos[2\pi f_0 x(22/32)]$$

$$+ 2\cos[2\pi f_0 x(26/32)] + 2\cos[2\pi f_0 x(30/32)] + 2\cos[2\pi f_0 x(34/32)]$$

$$+ 2\cos[2\pi f_0 x(38/32)] + 2\cos[2\pi f_0 x(42/32)] + 2\cos[2\pi f_0 x(46/32)]$$

$$+ 2\cos[2\pi f_0 x(50/32)] + 2\cos[2\pi f_0 x(54/32)] + 2\cos[2\pi f_0 x(58/32)]\}$$

$$\times [2(L - 2|x - L/2|)] \times \text{sinc}\{2(L - 2|x - L/2|) \times [f_x - f_0(4/64) - \beta x]\} (A19.30)$$

$$W_{Ia31}(x, f_x) = \{1 + 2\cos[2\pi f_0 x(4/32)] + 2\cos[2\pi f_0 x(8/32)] + 2\cos[2\pi f_0 x(12/32)]$$

$$+ 2\cos[2\pi f_0 x(16/32)] + 2\cos[2\pi f_0 x(20/32)] + 2\cos[2\pi f_0 x(24/32)]$$

$$+ 2\cos[2\pi f_0 x(28/32)] + 2\cos[2\pi f_0 x(32/32)] + 2\cos[2\pi f_0 x(36/32)]$$

$$+ 2\cos[2\pi f_0 x(40/32)] + 2\cos[2\pi f_0 x(44/32)] + 2\cos[2\pi f_0 x(48/32)]$$

$$+ 2\cos[2\pi f_0 x(52/32)] + 2\cos[2\pi f_0 x(56/32)] + 2\cos[2\pi f_0 x(60/32)]\}$$

$$\times [2(L - 2|x - L/2|)] \times \mathrm{sinc}\{2(L - 2|x - L/2|) \times [f_x - f_0(2/64) - \beta x]\} \quad \text{(A19.31)}$$

$$W_{Ia32}(x, f_x) = \{2\cos[2\pi f_0 x(2/32)] + 2\cos[2\pi f_0 x(6/32)] + 2\cos[2\pi f_0 x(10/32)]$$

$$+ 2\cos[2\pi f_0 x(14/32)] + 2\cos[2\pi f_0 x(18/32)] + 2\cos[2\pi f_0 x(22/32)]$$

$$+ 2\cos[2\pi f_0 x(26/32)] + 2\cos[2\pi f_0 x(30/32)] + 2\cos[2\pi f_0 x(34/32)]$$

$$+ 2\cos[2\pi f_0 x(38/32)] + 2\cos[2\pi f_0 x(42/32)] + 2\cos[2\pi f_0 x(46/32)]$$

$$+ 2\cos[2\pi f_0 x(50/32)] + 2\cos[2\pi f_0 x(54/32)] + 2\cos[2\pi f_0 x(58/32)]$$

$$+ 2\cos[2\pi f_0 x(62/32)]\} \times [2(L - 2|x - L/2|)]$$

$$\times \mathrm{sinc}\{2(L - 2|x - L/2|)(f_x - \beta x)\} \quad \text{(A19.32)}$$

$$W_{Ia33}(x, f_x) = \{1 + 2\cos[2\pi f_0 x(4/32)] + 2\cos[2\pi f_0 x(8/32)] + 2\cos[2\pi f_0 x(12/32)]$$

$$+ 2\cos[2\pi f_0 x(16/32)] + 2\cos[2\pi f_0 x(20/32)] + 2\cos[2\pi f_0 x(24/32)]$$

$$+ 2\cos[2\pi f_0 x(28/32)] + 2\cos[2\pi f_0 x(32/32)] + 2\cos[2\pi f_0 x(36/32)]$$

$$+ 2\cos[2\pi f_0 x(40/32)] + 2\cos[2\pi f_0 x(44/32)] + 2\cos[2\pi f_0 x(48/32)]$$

$$+ 2\cos[2\pi f_0 x(52/32)] + 2\cos[2\pi f_0 x(56/32)] + 2\cos[2\pi f_0 x(60/32)]\}$$

$$\times [2(L - 2|x - L/2|)] \times \mathrm{sinc}\{2(L - 2|x - L/2|) \times [f_x + f_0(2/64) - \beta x]\} \quad \text{(A19.33)}$$

$$W_{Ia34}(x, f_x) = \{2\cos[2\pi f_0 x(2/32)] + 2\cos[2\pi f_0 x(6/32)] + 2\cos[2\pi f_0 x(10/32)]$$

$$+ 2\cos[2\pi f_0 x(14/32)] + 2\cos[2\pi f_0 x(18/32)] + 2\cos[2\pi f_0 x(22/32)]$$

$$+\,2\cos[2\pi f_0 x(26/32)]+2\cos[2\pi f_0 x(30/32)]+2\cos[2\pi f_0 x(34/32)]$$

$$+\,2\cos[2\pi f_0 x(38/32)]+2\cos[2\pi f_0 x(42/32)]+2\cos[2\pi f_0 x(46/32)]$$

$$+\,2\cos[2\pi f_0 x(50/32)]+2\cos[2\pi f_0 x(54/32)]+2\cos[2\pi f_0 x(58/32)]\}$$

$$\times\,[2(L-2|x-L/2|)]\times\mathrm{sinc}\{2(L-2|x-L/2|)\times[f_x+f_0(4/64)-\beta x]\} \quad \text{(A19.34)}$$

$$W_{Ia35}(x,f_x)=\{1+2\cos[2\pi f_0 x(4/32)]+2\cos[2\pi f_0 x(8/32)]+2\cos[2\pi f_0 x(12/32)]$$

$$+\,2\cos[2\pi f_0 x(16/32)]+2\cos[2\pi f_0 x(20/32)]+2\cos[2\pi f_0 x(24/32)]$$

$$+\,2\cos[2\pi f_0 x(28/32)]+2\cos[2\pi f_0 x(32/32)]+2\cos[2\pi f_0 x(36/32)]$$

$$+\,2\cos[2\pi f_0 x(40/32)]+2\cos[2\pi f_0 x(44/32)]+2\cos[2\pi f_0 x(48/32)]$$

$$+\,2\cos[2\pi f_0 x(52/32)]+2\cos[2\pi f_0 x(56/32)]\}\times[2(L-2|x-L/2|)]$$

$$\times\,\mathrm{sinc}\{2(L-2|x-L/2|)[f_x+f_0(6/64)-\beta x]\} \quad \text{(A19.35)}$$

$$W_{Ia36}(x,f_x)=\{2\cos[2\pi f_0 x(2/32)]+2\cos[2\pi f_0 x(6/32)]+2\cos[2\pi f_0 x(10/32)]$$

$$+\,2\cos[2\pi f_0 x(14/32)]+2\cos[2\pi f_0 x(18/32)]+2\cos[2\pi f_0 x(22/32)]$$

$$+\,2\cos[2\pi f_0 x(26/32)]+2\cos[2\pi f_0 x(30/32)]+2\cos[2\pi f_0 x(34/32)]$$

$$+\,2\cos[2\pi f_0 x(38/32)]+2\cos[2\pi f_0 x(42/32)]+2\cos[2\pi f_0 x(46/32)]$$

$$+\,2\cos[2\pi f_0 x(50/32)]+2\cos[2\pi f_0 x(54/32)]\}\times[2(L-2|x-L/2|)]$$

$$\times\,\mathrm{sinc}\{2(L-2|x-L/2|)[f_x+f_0(8/64)-\beta x]\} \quad \text{(A19.36)}$$

$$W_{Ia37}(x,f_x)=\{1+2\cos[2\pi f_0 x(4/32)]+2\cos[2\pi f_0 x(8/32)]+2\cos[2\pi f_0 x(12/32)]$$

$$+\,2\cos[2\pi f_0 x(16/32)]+2\cos[2\pi f_0 x(20/32)]+2\cos[2\pi f_0 x(24/32)]$$

$$+ 2\cos[2\pi f_0 x(28/32)] + 2\cos[2\pi f_0 x(32/32)] + 2\cos[2\pi f_0 x(36/32)]$$

$$+ 2\cos[2\pi f_0 x(40/32)] + 2\cos[2\pi f_0 x(44/32)] + 2\cos[2\pi f_0 x(48/32)]$$

$$+ 2\cos(2\pi f_0 x(52/32))\} \times [2(L - 2|x - L/2|)]$$

$$\times \mathrm{sinc}\{2(L - 2|x - L/2|) \times [f_x + f_0(10/64) - \beta x]\} \qquad (A19.37)$$

$$W_{Ia38}(x, f_x) = \{2\cos[2\pi f_0 x(2/32)] + 2\cos[2\pi f_0 x(6/32)] + 2\cos[2\pi f_0 x(10/32)]$$

$$+ 2\cos[2\pi f_0 x(14/32)] + 2\cos[2\pi f_0 x(18/32)] + 2\cos[2\pi f_0 x(22/32)]$$

$$+ 2\cos[2\pi f_0 x(26/32)] + 2\cos[2\pi f_0 x(30/32)] + 2\cos[2\pi f_0 x(34/32)]$$

$$+ 2\cos[2\pi f_0 x(38/32)] + 2\cos[2\pi f_0 x(42/32)] + 2\cos[2\pi f_0 x(46/32)]$$

$$+ 2\cos[2\pi f_0 x(50/32)]\} \times [2(L - 2|x - L/2|)]$$

$$\times \mathrm{sinc}\{2(L - 2|x - L/2|) \times [f_x + f_0(12/64) - \beta x]\} \qquad (A19.38)$$

$$W_{Ia39}(x, f_x) = \{1 + 2\cos[2\pi f_0 x(4/32)] + 2\cos[2\pi f_0 x(8/32)] + 2\cos[2\pi f_0 x(12/32)]$$

$$+ 2\cos[2\pi f_0 x(16/32)] + 2\cos[2\pi f_0 x(20/32)] + 2\cos[2\pi f_0 x(24/32)]$$

$$+ 2\cos[2\pi f_0 x(28/32)] + 2\cos[2\pi f_0 x(32/32)] + 2\cos[2\pi f_0 x(36/32)]$$

$$+ 2\cos[2\pi f_0 x(40/32)] + 2\cos[2\pi f_0 x(44/32)] + 2\cos[2\pi f_0 x(48/32)]\}$$

$$\times [2(L - 2|x - L/2|)] \times \mathrm{sinc}\{2(L - 2|x - L/2|) \times [f_x + f_0(14/64) - \beta x]\} \quad (A19.39)$$

$$W_{Ia40}(x, f_x) = \{2\cos[2\pi f_0 x(2/32)] + 2\cos[2\pi f_0 x(6/32)] + 2\cos[2\pi f_0 x(10/32)]$$

$$+ 2\cos[2\pi f_0 x(14/32)] + 2\cos[2\pi f_0 x(18/32)] + 2\cos[2\pi f_0 x(22/32)]$$

$$+ 2\cos[2\pi f_0 x(26/32)] + 2\cos[2\pi f_0 x(30/32)] + 2\cos[2\pi f_0 x(34/32)]$$

$$+ 2\cos[2\pi f_0 x(38/32)] + 2\cos[2\pi f_0 x(42/32)] + 2\cos[2\pi f_0 x(46/32)]\}$$

$$\times [2(L - 2|x - L/2|)] \times \text{sinc}\{2(L - 2|x - L/2|) \times [f_x + f_0(16/64) - \beta x]\} \quad \text{(A19.40)}$$

$$W_{Ia41}(x, f_x) = \{1 + 2\cos[2\pi f_0 x(4/32)] + 2\cos[2\pi f_0 x(8/32)] + 2\cos[2\pi f_0 x(12/32)]$$

$$+ 2\cos[2\pi f_0 x(16/32)] + 2\cos[2\pi f_0 x(20/32)] + 2\cos[2\pi f_0 x(24/32)]$$

$$+ 2\cos[2\pi f_0 x(28/32)] + 2\cos[2\pi f_0 x(32/32)] + 2\cos[2\pi f_0 x(36/32)]$$

$$+ 2\cos[2\pi f_0 x(40/32)] + 2\cos[2\pi f_0 x(44/32)]\} \times [2(L - 2|x - L/2|)]$$

$$\times \text{sinc}\{2(L - 2|x - L/2|) \times [f_x + f_0(18/64) - \beta x]\} \quad \text{(A19.41)}$$

$$W_{Ia42}(x, f_x) = \{2\cos[2\pi f_0 x(2/32)] + 2\cos[2\pi f_0 x(6/32)] + 2\cos[2\pi f_0 x(10/32)]$$

$$+ 2\cos[2\pi f_0 x(14/32)] + 2\cos[2\pi f_0 x(18/32)] + 2\cos[2\pi f_0 x(22/32)]$$

$$+ 2\cos[2\pi f_0 x(26/32)] + 2\cos[2\pi f_0 x(30/32)] + 2\cos[2\pi f_0 x(34/32)]$$

$$+ 2\cos[2\pi f_0 x(38/32)] + 2\cos[2\pi f_0 x(42/32)]\} \times [2(L - 2|x - L/2|)]$$

$$\times \text{sinc}\{2(L - 2|x - L/2|) \times [f_x + f_0(20/64) - \beta x]\} \quad \text{(A19.42)}$$

$$W_{Ia43}(x, f_x) = \{1 + 2\cos[2\pi f_0 x(4/32)] + 2\cos[2\pi f_0 x(8/32)] + 2\cos[2\pi f_0 x(12/32)]$$

$$+ 2\cos[2\pi f_0 x(16/32)] + 2\cos[2\pi f_0 x(20/32)] + 2\cos[2\pi f_0 x(24/32)]$$

$$+ 2\cos[2\pi f_0 x(28/32)] + 2\cos[2\pi f_0 x(32/32)] + 2\cos[2\pi f_0 x(36/32)]$$

$$+ 2\cos[2\pi f_0 x(40/32)]\} \times [2(L - 2|x - L/2|)]$$

$$\times \text{sinc}\{2(L - 2|x - L/2|) \times [f_x + f_0(22/64) - \beta x]\} \quad \text{(A19.43)}$$

$$W_{Ia44}(x, f_x) = \{2\cos[2\pi f_0 x(2/32)] + 2\cos[2\pi f_0 x(6/32)] + 2\cos[2\pi f_0 x(10/32)]$$

$$+ 2\cos[2\pi f_0 x(14/32)] + 2\cos[2\pi f_0 x(18/32)] + 2\cos[2\pi f_0 x(22/32)]$$

$$+ 2\cos[2\pi f_0 x(26/32)] + 2\cos[2\pi f_0 x(30/32)] + 2\cos[2\pi f_0 x(34/32)]$$

$$+ 2\cos[2\pi f_0 x(38/32)]\} \times [2(L - 2|x - L/2|)]$$

$$\times \operatorname{sinc}\{2(L - 2|x - L/2|) \times [f_x + f_0(24/64) - \beta x]\} \qquad \text{(A19.44)}$$

$$W_{Ia45}(x, f_x) = \{1 + 2\cos[2\pi f_0 x(4/32)] + 2\cos[2\pi f_0 x(8/32)] + 2\cos[2\pi f_0 x(12/32)]$$

$$+ 2\cos[2\pi f_0 x(16/32)] + 2\cos[2\pi f_0 x(20/32)] + 2\cos[2\pi f_0 x(24/32)]$$

$$+ 2\cos[2\pi f_0 x(28/32)] + 2\cos[2\pi f_0 x(32/32)] + 2\cos[2\pi f_0 x(36/32)]\}$$

$$\times [2(L - 2|x - L/2|)] \times \operatorname{sinc}\{2(L - 2|x - L/2|) \times [f_x + f_0(26/64) - \beta x]\} \quad \text{(A19.45)}$$

$$W_{Ia46}(x, f_x) = \{2\cos[2\pi f_0 x(2/32)] + 2\cos[2\pi f_0 x(6/32)] + 2\cos[2\pi f_0 x(10/32)]$$

$$+ 2\cos[2\pi f_0 x(14/32)] + 2\cos[2\pi f_0 x(18/32)] + 2\cos[2\pi f_0 x(22/32)]$$

$$+ 2\cos[2\pi f_0 x(26/32)] + 2\cos[2\pi f_0 x(30/32)] + 2\cos[2\pi f_0 x(34/32)]\}$$

$$\times [2(L - 2|x - L/2|)] \times \operatorname{sinc}\{2(L - 2|x - L/2|) \times [f_x + f_0(28/64) - \beta x]\} \quad \text{(A19.46)}$$

$$W_{Ia47}(x, f_x) = \{1 + 2\cos[2\pi f_0 x(4/32)] + 2\cos[2\pi f_0 x(8/32)] + 2\cos[2\pi f_0 x(12/32)]$$

$$+ 2\cos[2\pi f_0 x(16/32)] + 2\cos[2\pi f_0 x(20/32)] + 2\cos[2\pi f_0 x(24/32)]$$

$$+ 2\cos[2\pi f_0 x(28/32)] + 2\cos[2\pi f_0 x(32/32)]\} \times [2(L - 2|x - L/2|)]$$

$$\times \operatorname{sinc}\{2(L - 2|x - L/2|) \times [f_x + f_0(30/64) - \beta x]\} \qquad \text{(A19.47)}$$

$$W_{Ia48}(x, f_x) = \{2\cos[2\pi f_0 x(2/32)] + 2\cos[2\pi f_0 x(6/32)] + 2\cos[2\pi f_0 x(10/32)]$$

$$+ 2\cos[2\pi f_0 x(14/32)] + 2\cos[2\pi f_0 x(18/32)] + 2\cos[2\pi f_0 x(22/32)]$$

$$+ 2\cos[2\pi f_0 x(26/32)] + 2\cos[2\pi f_0 x(30/32)]\} \times [2(L - 2|x - L/2|)]$$

$$\times \operatorname{sinc}\{2(L - 2|x - L/2|) \times [f_x + f_0(32/64) - \beta x]\} \qquad \text{(A19.48)}$$

$$W_{Ia49}(x, f_x) = \{1 + 2\cos[2\pi f_0 x(4/32)] + 2\cos[2\pi f_0 x(8/32)] + 2\cos[2\pi f_0 x(12/32)]$$

$$+ 2\cos[2\pi f_0 x(16/32)] + 2\cos[2\pi f_0 x(20/32)] + 2\cos[2\pi f_0 x(24/32)]$$

$$+ 2\cos[2\pi f_0 x(28/32)]\} \times [2(L - 2|x - L/2|)]$$

$$\times \operatorname{sinc}\{2(L - 2|x - L/2|) \times [f_x + f_0(34/64) - \beta x]\} \qquad \text{(A19.49)}$$

$$W_{Ia50}(x, f_x) = \{2\cos[2\pi f_0 x(2/32)] + 2\cos[2\pi f_0 x(6/32)] + 2\cos[2\pi f_0 x(10/32)]$$

$$+ 2\cos[2\pi f_0 x(14/32)] + 2\cos[2\pi f_0 x(18/32)] + 2\cos[2\pi f_0 x(22/32)]$$

$$+ 2\cos[2\pi f_0 x(26/32)]\} \times [2(L - 2|x - L/2|)]$$

$$\times \operatorname{sinc}\{2(L - 2|x - L/2|) \times [f_x + f_0(36/64) - \beta x]\} \qquad \text{(A19.50)}$$

$$W_{Ia51}(x, f_x) = \{1 + 2\cos[2\pi f_0 x(4/32)] + 2\cos[2\pi f_0 x(8/32)] + 2\cos[2\pi f_0 x(12/32)]$$

$$+ 2\cos[2\pi f_0 x(16/32)] + 2\cos[2\pi f_0 x(20/32)] + 2\cos[2\pi f_0 x(24/32)]\}$$

$$\times [2(L - 2|x - L/2|)] \times \operatorname{sinc}\{2(L - 2|x - L/2|) \times [f_x + f_0(38/64) - \beta x]\} \text{ (A19.51)}$$

$$W_{Ia52}(x, f_x) = \{2\cos[2\pi f_0 x(2/32)] + 2\cos[2\pi f_0 x(6/32)] + 2\cos[2\pi f_0 x(10/32)]$$

$$+ 2\cos[2\pi f_0 x(14/32)] + 2\cos[2\pi f_0 x(18/32)] + 2\cos[2\pi f_0 x(22/32)]\}$$

$$\times [2(L-2|x-L/2|)] \times \mathrm{sinc}\{2(L-2|x-L/2|) \times [f_x + f_0(40/64) - \beta x]\} \quad \text{(A19.52)}$$

$$W_{Ia53}(x, f_x) = \{1 + 2\cos[2\pi f_0 x(4/32)] + 2\cos[2\pi f_0 x(8/32)] + 2\cos[2\pi f_0 x(12/32)]$$
$$+ 2\cos[2\pi f_0 x(16/32)] + 2\cos[2\pi f_0 x(20/32)]\} \times [2(L-2|x-L/2|)]$$
$$\times \mathrm{sinc}\{2(L-2|x-L/2|) \times [f_x + f_0(42/64) - \beta x]\} \quad \text{(A19.53)}$$

$$W_{Ia54}(x, f_x) = \{2\cos[2\pi f_0 x(2/32)] + 2\cos[2\pi f_0 x(6/32)] + 2\cos[2\pi f_0 x(10/32)]$$
$$+ 2\cos[2\pi f_0 x(14/32)] + 2\cos[2\pi f_0 x(18/32)]\} \times [2(L-2|x-L/2|)]$$
$$\times \mathrm{sinc}\{2(L-2|x-L/2|) \times [f_x + f_0(44/64) - \beta x]\} \quad \text{(A19.54)}$$

$$W_{Ia55}(x, f_x) = \{1 + 2\cos[2\pi f_0 x(4/32)] + 2\cos[2\pi f_0 x(8/32)] + 2\cos[2\pi f_0 x(12/32)]$$
$$+ 2\cos[2\pi f_0 x(16/32)]\} \times [2(L-2|x-L/2|)]$$
$$\times \mathrm{sinc}\{2(L-2|x-L/2|) \times [f_x + f_0(46/64) - \beta x]\} \quad \text{(A19.55)}$$

$$W_{Ia56}(x, f_x) = \{2\cos[2\pi f_0 x(2/32)] + 2\cos[2\pi f_0 x(6/32)] + 2\cos[2\pi f_0 x(10/32)]$$
$$+ 2\cos[2\pi f_0 x(14/32)]\} \times [2(L-2|x-L/2|)]$$
$$\times \mathrm{sinc}\{2(L-2|x-L/2|) \times [f_x + f_0(48/64) - \beta x]\} \quad \text{(A19.56)}$$

$$W_{Ia57}(x, f_x) = \{1 + 2\cos[2\pi f_0 x(4/32)] + 2\cos[2\pi f_0 x(8/32)] + 2\cos[2\pi f_0 x(12/32)]\}$$
$$\times [2(L-2|x-L/2|)] \times \mathrm{sinc}\{2(L-2|x-L/2|) \times [f_x + f_0(50/64) - \beta x]\} \quad \text{(A19.57)}$$

$$W_{Ia58}(x, f_x) = \{2\cos[2\pi f_0 x(2/32)] + 2\cos[2\pi f_0 x(6/32)] + 2\cos[2\pi f_0 x(10/32)]\}$$
$$\times [2(L - 2|x - L/2|)] \times \mathrm{sinc}\{2(L - 2|x - L/2|) \times [f_x + f_0(52/64) - \beta x]\} \quad \text{(A19.58)}$$

$$W_{Ia59}(x, f_x) = \{1 + 2\cos(2\pi f_0 x(4/32)) + 2\cos(2\pi f_0 x(8/32))\} \times [2(L - 2|x - L/2|)]$$
$$\times \mathrm{sinc}\{2(L - 2|x - L/2|) \times [f_x + f_0(54/64) - \beta x]\} \quad \text{(A19.59)}$$

$$W_{Ia60}(x, f_x) = \{2\cos[2\pi f_0 x(2/32)] + 2\cos[2\pi f_0 x(6/32)]\} \times [2(L - 2|x - L/2|)]$$
$$\times \mathrm{sinc}\{2(L - 2|x - L/2|) \times [f_x + f_0(56/64) - \beta x]\} \quad \text{(A19.60)}$$

$$W_{Ia61}(x, f_x) = [1 + 2\cos[2\pi f_0 x(4/32)]] \times [2(L - 2|x - L/2|)]$$
$$\times \mathrm{sinc}\{2(L - 2|x - L/2|) \times [f_x + f_0(58/64) - \beta x]\} \quad \text{(A19.61)}$$

$$W_{Ia62}(x, f_x) = 2\cos[2\pi f_0 x(2/32)] \times [2(L - 2|x - L/2|)]$$
$$\times \mathrm{sinc}\{2(L - 2|x - L/2|) \times [f_x + f_0(60/64) - \beta x]\} \quad \text{(A19.62)}$$

$$W_{Ia63}(x, f_x) = \mathrm{sinc}\{2(L - 2|x - L/2|) \times [f_x + f_0(62/64) - \beta x]\}$$
$$\times [2(L - 2|x - L/2|)]. \quad \text{(A19.63)}$$

CURRICULUM VITAE

Miss Porntip Chuamchaitrakool received her B.Eng. degree in electrical engineering and M.Eng. degree in mechanical engineering from Suranaree University of Technology, Thailand, in 2002 and 2011, respectively. In 2012, she decided to pursue her Ph.D. study in school of physics (laser program) at the same university under the supervision of Professor Dr. Joewono Widjaja and was granted the Royal Golden Jubilee Ph.D. Program scholarship (Grant No. PHD/0114/2554). Owing to this scholarship, she had the academic experience as a Ph.D. researcher at Chiba University, Chiba prefecture, Japan under the supervision of her co-advisor, Associate Professor Dr. Hiroyuki Yoshimura. During her Ph.D. study, her researches were presented and won for the outstanding poster presentation award and the outstanding oral presentation award in the Congress on Science and Technology of Thailand (STT 41) 2015 and the RGJ-Ph.D. Congress XVII 2016, respectively. Her current research interests are digital holography and digital signal processing.